Precision Continuum Receivers for Astrophysical Applications

Edward J. Wollack
NASA Goddard Space Flight Center
Greenbelt MD, 20771

RadioNet FP7 “Receiver Gain Stability” Workshop
Cagliari, Sardinian, Italy

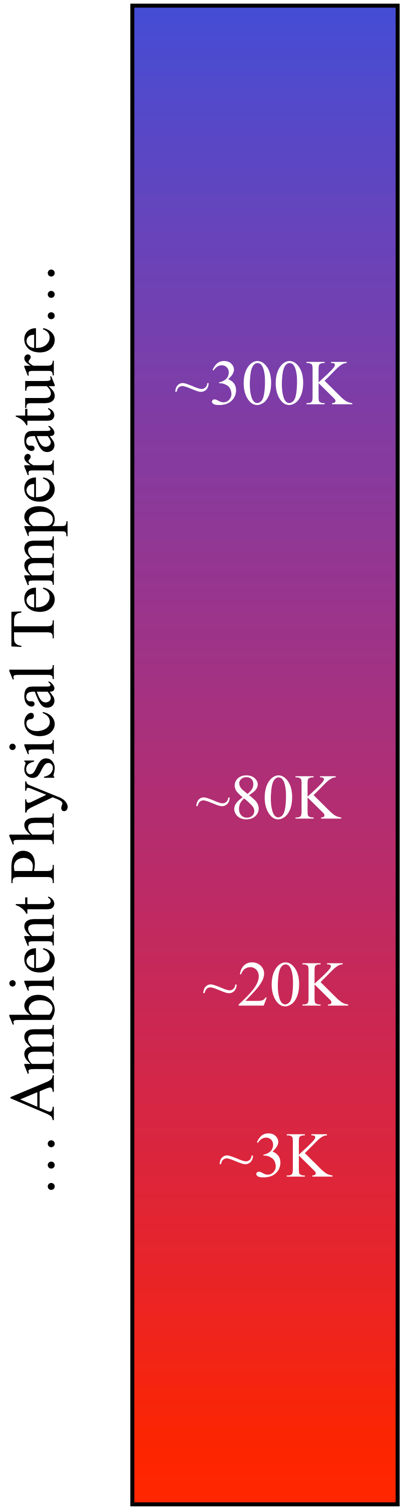

Low-Noise HFET Applications…

- **Communications:**
  - Direct Broadcast Satellite…
  - Receiver IF Backend…
  - Secure Communication Links…

  …
- **Instrumentation:**
- **Imaging and Detection:**
  - Remote Sensing…
  - Contraband Detection…
  - Collision Avoidance Radar…
  - Smart Munition Sensors…

  …
- **Thermal Electrically Cooled Satellite Ground Stations**

  …
- **Passively Cooled Satellite Receivers**

  …
- **Actively Cooled Receiver Systems**
  - Deep Space Network Receivers…
  - Radio Astronomy…
    - Low-Noise Broad-Band Radiometers…
    - Low-Noise Receiver Frontends…
    - Low-Noise Receiver Backends…

  …
- **Low-Noise Detector Applications**
    - Direct Power Detection, Heterodyne Front-Ends, SIS Mixer IF amplifier…
    - Kinetic Inductance Bolometic Readout…
    - Low-Noise Electrometer Readout, Johnson Noise Thermometry…
    - Particle Accelerator Beam Monitor (Stochastic Cooling)…
    - Gravitational Wave and Axion Detector Readouts…

  …

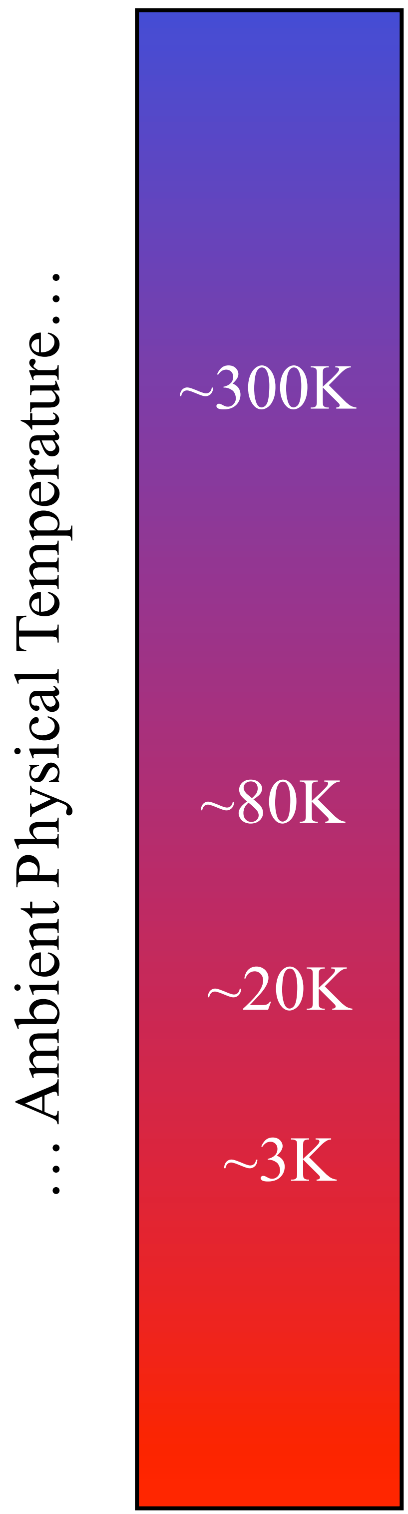

Low-Noise HFET Applications…

- **Communications:**
  - Direct Broadcast Satellite…
  - Receiver IF Backend…
  - Secure Communication Links…

  …
- **Instrumentation:**
- **Imaging and Detection:**
  - Remote Sensing…
  - Contraband Detection…
  - Collision Avoidance Radar…
  - Smart Munition Sensors…

  …
- **Thermal Electrically Cooled Satellite Ground Stations**

  …
- **Passively Cooled Satellite Receivers**

  …
- **Actively Cooled Receiver Systems**
  - Deep Space Network Receivers…
  - Radio Astronomy…
    - Low-Noise Broad-Band Radiometers…
    - Low-Noise Receiver Frontends…
    - Low-Noise Receiver Backends…

  …
- **Low-Noise Detector Applications**
    - Direct Power Detection, Heterodyne Front-Ends, SIS Mixer IF amplifier…
    - Kinetic Inductance Bolometic Readout…
    - Low-Noise Electrometer Readout, Johnson Noise Thermometry…
    - Particle Accelerator Beam Monitor (Stochastic Cooling)…
    - Gravitational Wave and Axion Detector Readouts…

  …

Require Knowledge of Performance…
- Average: Noise, Gain, Phase
- Variation/Sensitivity: Amplitude, Phase

Device Stability: *'1/f'* - Noise

- Device Configuration and Material Contributions:
  - Trap Density and Location…
  - Surface Passivation, Interface Quality, Material Stability…
  - Device Environmental Bias Sensitivities…
    - Gate/Drain/Source Relative Electrical Bias
    - Thermal, Ambient Magnetic Field…
    - Electromagnetic/Particle/Radiation Exposure…
    - Package Environment and Integrity…
- Receiver Design Considerations:
  - Topology/Configuration (e.g. correlation vs. total power)
  - RF Bandwidth, Modulation Rate, Radiometric Offset…
  - Scan and Calibration Rates, Observation Interconnectivity…
- Mathematically: Sensor has Memory or Feedback
  - "Popcorn" or distribution of time scales → *1/f* but time domain differ
  - Intrinsic device *1/f* can easily be masked by other issues…
  - Lack of a well defined mean value – challenge for end user…

*…given the **intrinsic** detector's behavior our goal is provide a suitable environment and receiver architecture which achieves near optimal radiometric imaging performance…*

Beam Switched Total Power Receiver…

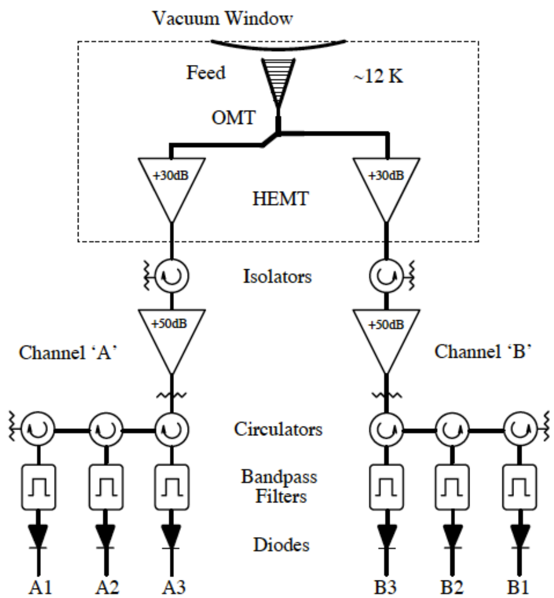

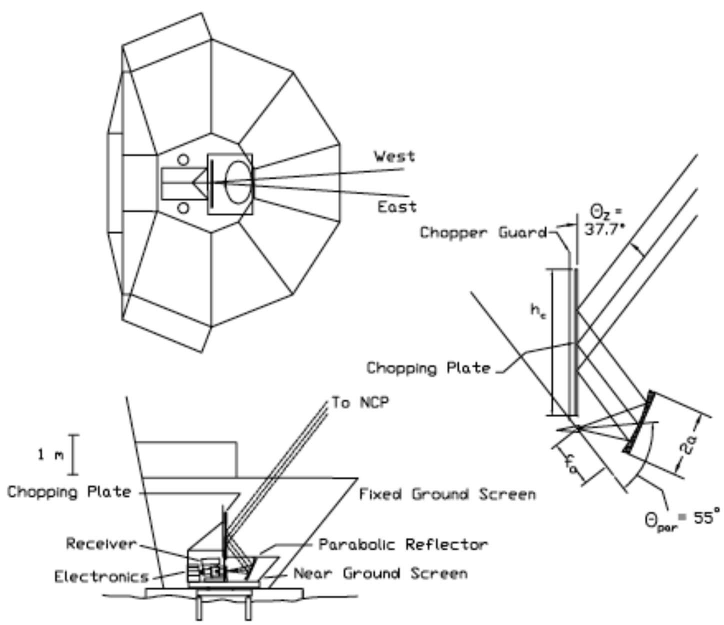

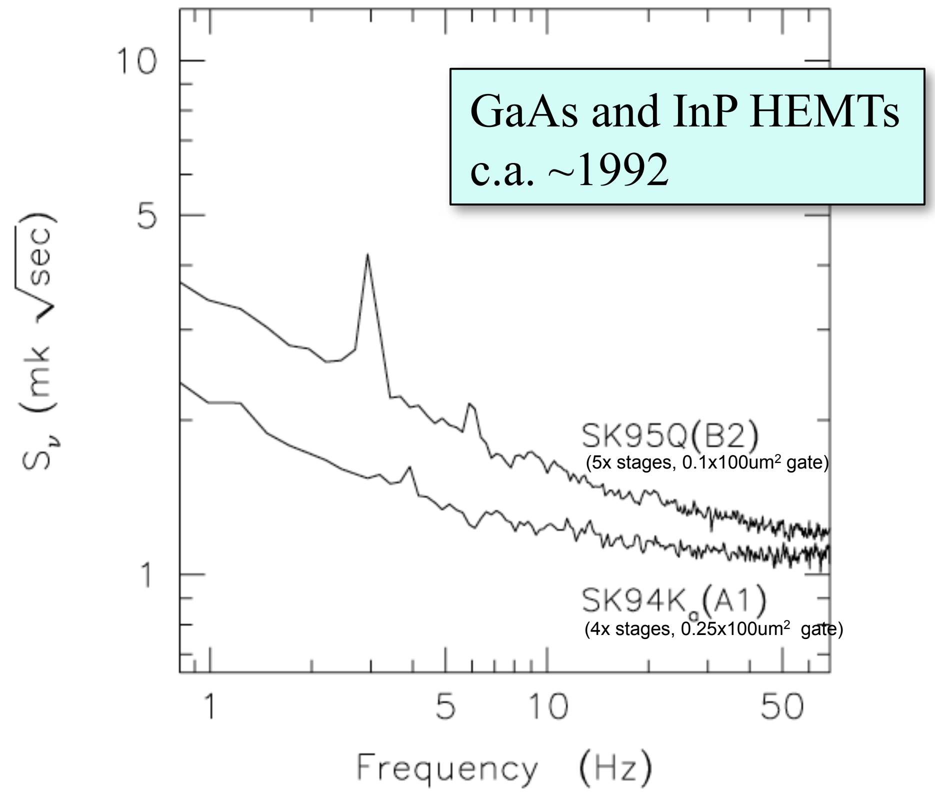

FIG. 3.—Typical power spectra, S_ν, of the receiver output. The data were taken while observing the sky during good weather. For SK95Q, the two-point and three-point offsets (see §§ 4.1 and 5) are manifest as the spectral features at 3 and 6 Hz ($\zeta < 1.5$ mK s$^{1/2}$ deg^{-1}). For SK94K$_a$, only the two-point offset at 4 Hz is evident ($\zeta < 0.9$ mK s$^{1/2}$ deg^{-1}). Data taken under laboratory conditions have an indistinguishable $1/f$ component that originates from the cooled HEMTs. Given the approximately equal bandwidths in the K$_a$ and Q systems, the higher Q-band $1/f$ knee reflects a lower gain stability. At $f \gg 100$ Hz the power spectra for both radiometers agree with the sensitivity derived from the measured RF bandwidth and system temperature. At 8 Hz, these results may be compared to $S_{\rm sky}$ in Table 3. The slight differences between the plot and the table result from the atmospheric noise contribution.

Wollack, E.J., *et al*, "An Instrument for Investigation of the Cosmic Microwave Background Radiation at Intermediate Angular Scales", 1997 *ApJ,* 476

Total Power Receiver - HEMT Characterization…

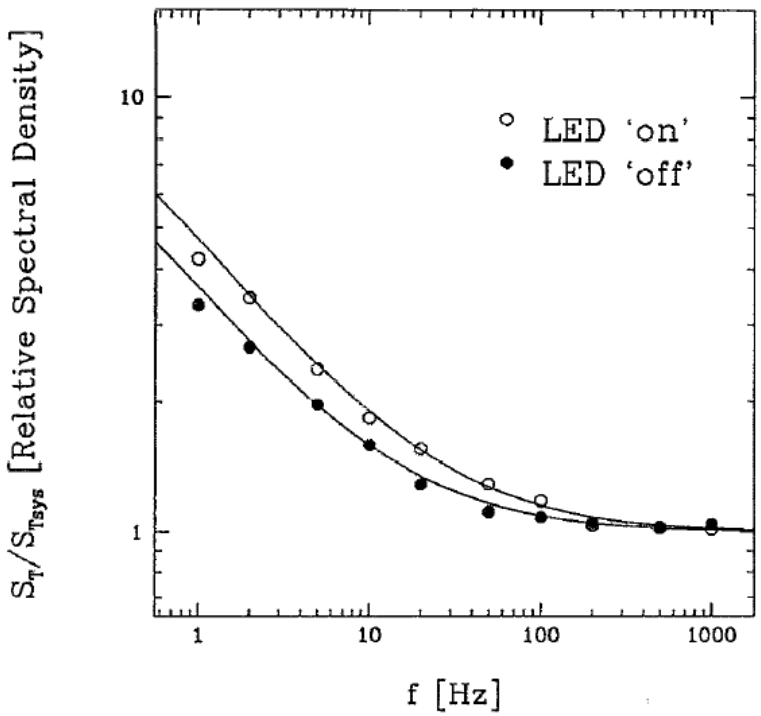

FIG. 2. The measured spectral density of NRAO amplifier B11 at physical temperature, $T_{amb}=18$ K. The data are normalized to the spectral density at 5 kHz. Filled and unfilled symbols indicate measurements taken with the amplifier's light-emitting diode respectively in the off and on states. No measurable difference in the rf noise or gain was noted upon energizing the LEDs. The best fit spectral index of the $1/f^{\alpha}$ component of the recorded data is $\alpha=0.9\pm0.1$. Within the measurement errors α is independent of LED illumination status. The best fit magnitude of the $1/f$ component of the noise spectrum was noted to increase by ~35% upon illuminating the amplifier HEMTs with the LED lamps.

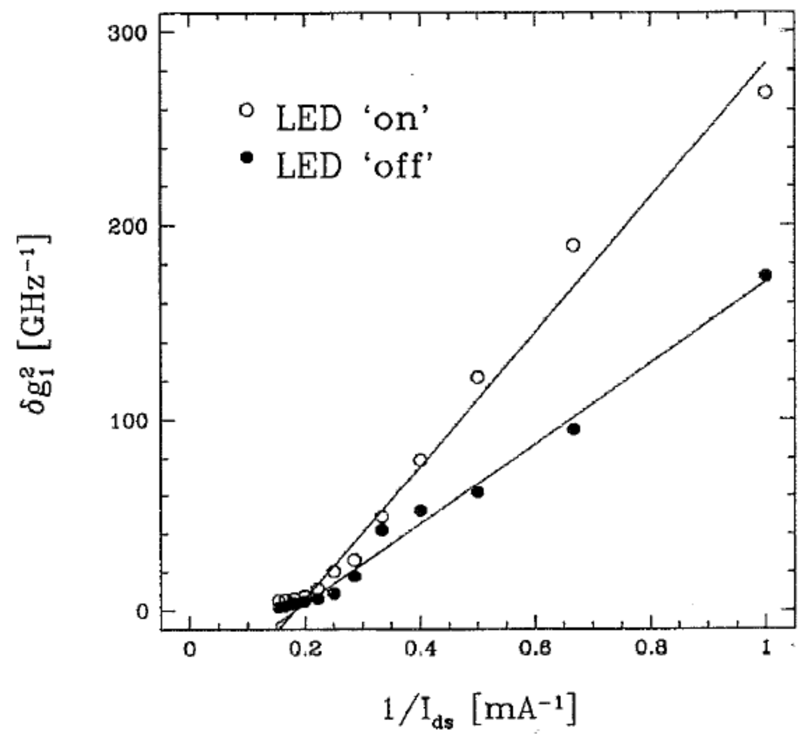

FIG. 3. The variation in the amplifier gain spectral density at physical temperature $T_{amb}=18$ K as a function of source-drain current. In this test, all five stages of amplifier B11 were set at I_{ds} and the magnitude of the amplifier gain fluctuation spectral density was recorded. Filled and unfilled symbols indicate measurements taken with the amplifier's light emitting diode, respectively, in the off and on states. For the amplifier under test, the variation in the effective rf bandwidth was a perturbation on the change in δg_1^2 as a function of drain current.

Conclusion: *Device changes which lead to noise/gain improvements can potentially degrade amplifier stability – rethink architecture for broadband radiometry…*

Wollack, E.J., "High-Electron-Mobility-Transistor Gain Stability and its Design Implications for Wide Band Millimeter Wave Receivers," 1995, Review of Scientific Instruments, Vol. 66(8), pp. 4305-4312.

Total Power Receiver - HEMT Characterization…

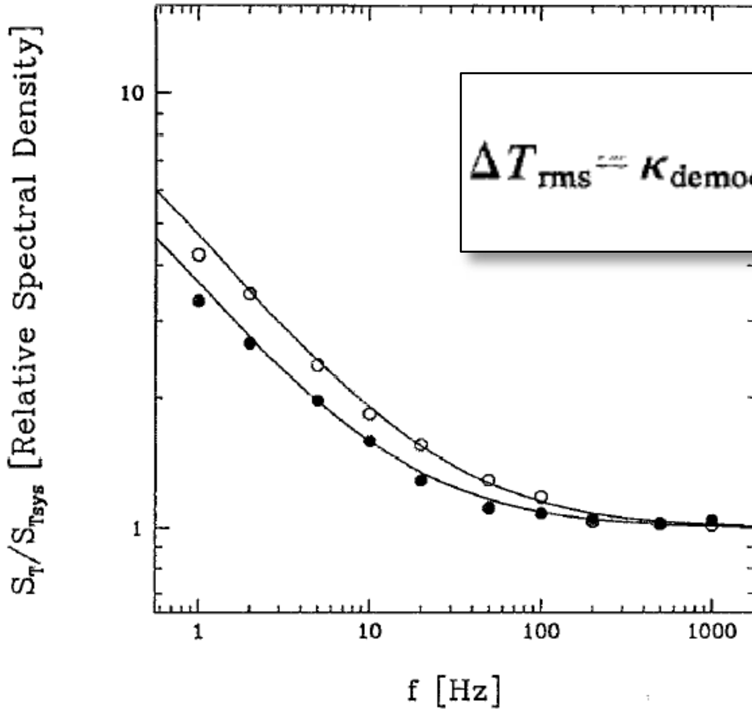

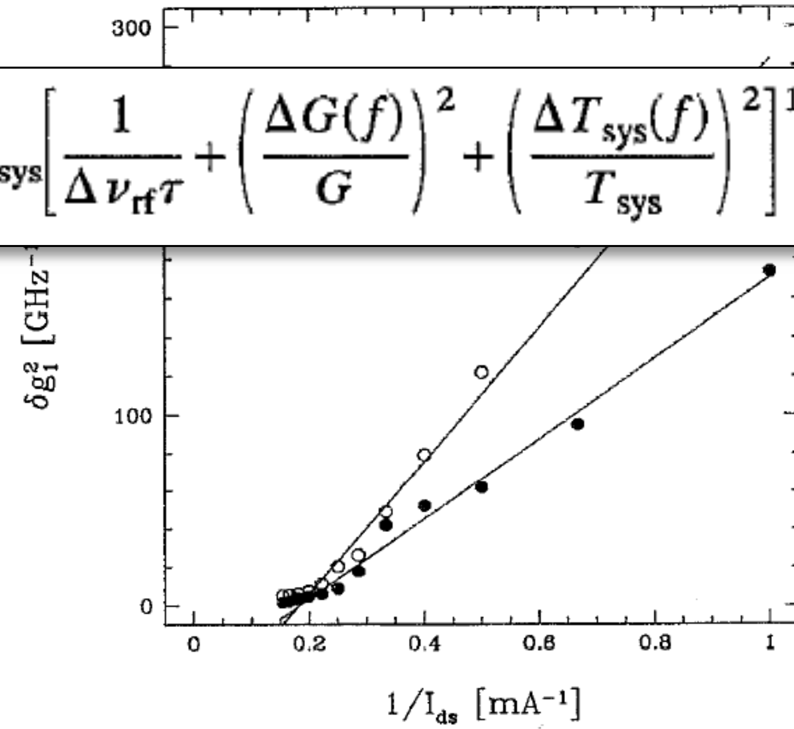

$$\Delta T_{rms} = \kappa_{demod} T_{sys} \left[\frac{1}{\Delta \nu_{rf} \tau} + \left(\frac{\Delta G(f)}{G} \right)^2 + \left(\frac{\Delta T_{sys}(f)}{T_{sys}} \right)^2 \right]^{1/2}$$

FIG. 2. The measured spectral density of NRAO amplifier B11 at physical
temperature, T_{amb}=18 K. The data are norma
5 kHz. Filled and unfilled symbols indicate
amplifier's light-emitting diode respectively
measurable difference in the rf noise or gain
LEDs. The best fit spectral index of the $1/f^\alpha$ c
is α=0.9±0.1. Within the measurement err
illumination status. The best fit magnitude of
spectrum was noted to increase by ~35% u
HEMTs with the LED lamps.

FIG. 3. The variation in the amplifier gain spectral density at physical tem-

Observation: Low frequency fluctuations intrinsic to the device modulate the effective bias point and appear as up-converted gain variations in the RF output of the amplifier – the end effect is an increase in the observed noise spectra.

Conclusion: *Device changes which lead to noise/gain improvements can potentially degrade amplifier stability – rethink architecture for broadband radiometry…*

Wollack, E.J., "High-Electron-Mobility-Transistor Gain Stability and its Design Implications for Wide Band Millimeter Wave Receivers," 1995, Review of Scientific Instruments, Vol. 66(8), pp. 4305-4312.

Total Power Receiver - Software Cross-Correlation…

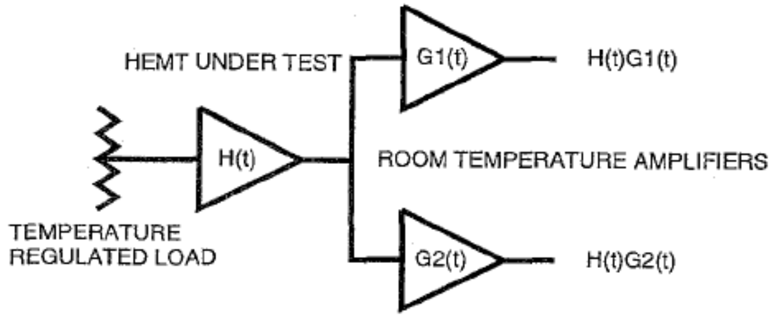

Fig. 1. Simplified model of the radiometer used to explain the correlation technique.

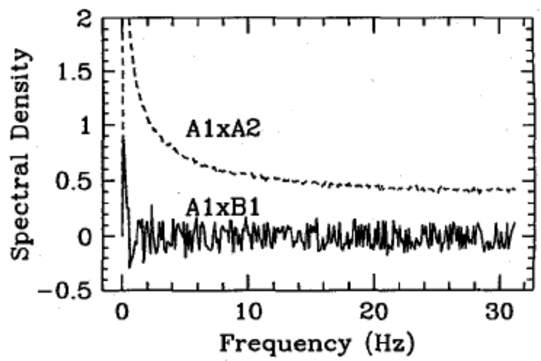

Fig. 4. Spectral density of the power fluctuations obtained from the cross-correlations $A1 \times A2$ (dashed) and $A1 \times B1$ (solid) with the radiometer configured as in Fig. 2.

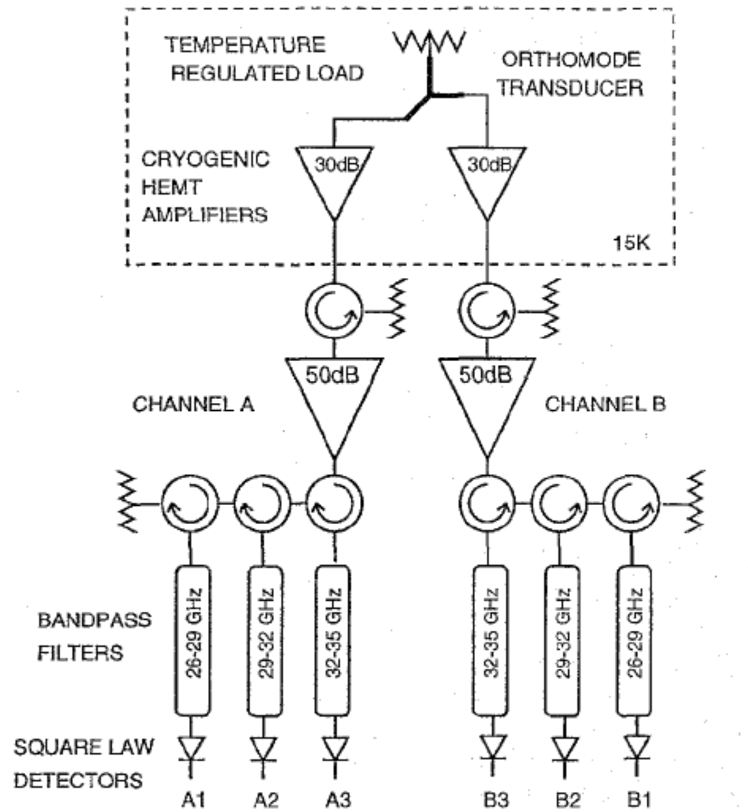

Fig. 2. Detailed block diagram of the radiometer employed in these measurements. The items enclosed in the dashed box were cooled to ~ 15 K by a closed cycle helium refrigerator.

Jarosik, N., et al., “Measurements of the Low Frequency Noise Properties of a 30 GHz High-Electron-Mobility-Transistor Amplifier,” June 1993, Princeton University Physics, Technical Report.

Jarosik, N. “Measurements of the low-frequency-gain fluctuations of a 30-GHz high-electron-mobility-transistor cryogenic amplifier”, 1996, IEEE Transactions on Microwave Theory and Techniques, Vol. 44, No. 2, pp. 193-197.

Total Power Receiver - Software Cross-Correlation…

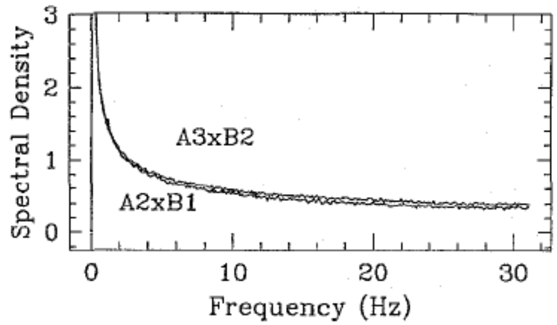

Fig. 7. Spectral density of the power fluctuations obtained from the cross-correlation between different frequency bands of the two radiometer channels, $A3 \times B2$ and $A2 \times B1$.

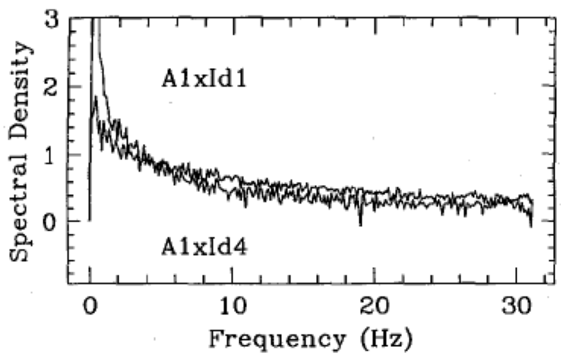

Fig. 9. Cross-correlations between the output power of radiometer channel $A1$ and the drain current of the input transistor of the HEMT amplifier $(A1 \times I_{d1})$ and the drain current of the final transistor of the HEMT amplifier $(A1 \times I_{d4})$.

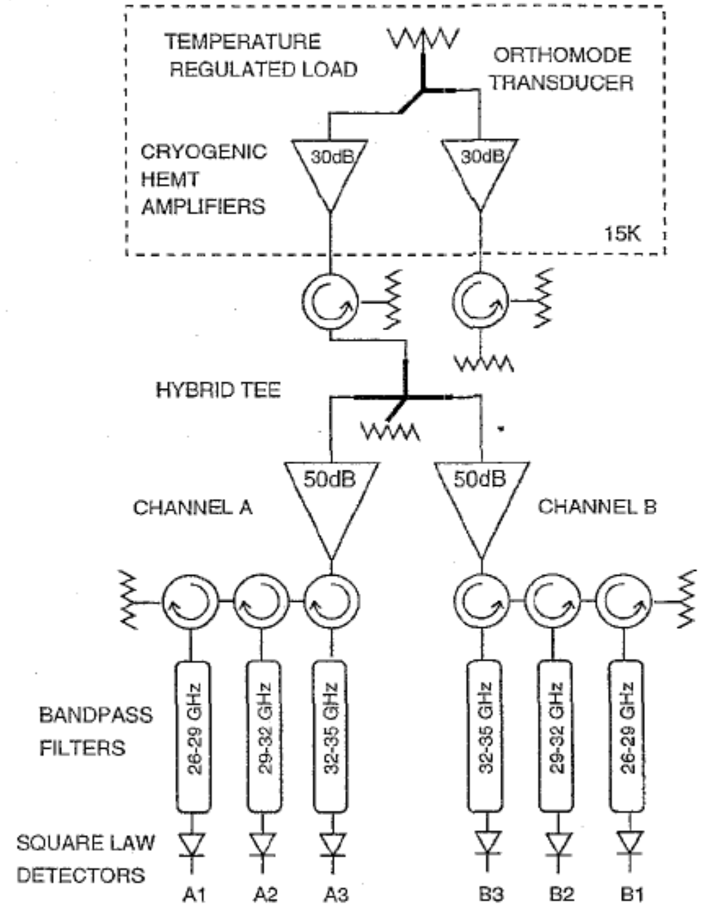

Fig. 5. The radiometer as configured to measure the HEMT amplifier's characteristics.

$$\rho_{\delta g\, i_d} = \left.\frac{\langle \delta g \cdot \delta i_d \rangle}{\sqrt{\langle \delta g^2 \rangle \langle \delta {i_d}^2 \rangle}}\right| \sim 0.3$$

Jarosik, N. "Measurements of the low-frequency-gain fluctuations of a 30-GHz high-electron-mobility-transistor cryogenic amplifier", 1996, IEEE Transactions on Microwave Theory and Techniques, Vol. 44, No. 2, pp. 193-197.

Total Power Receiver - Software Cross-Correlation…

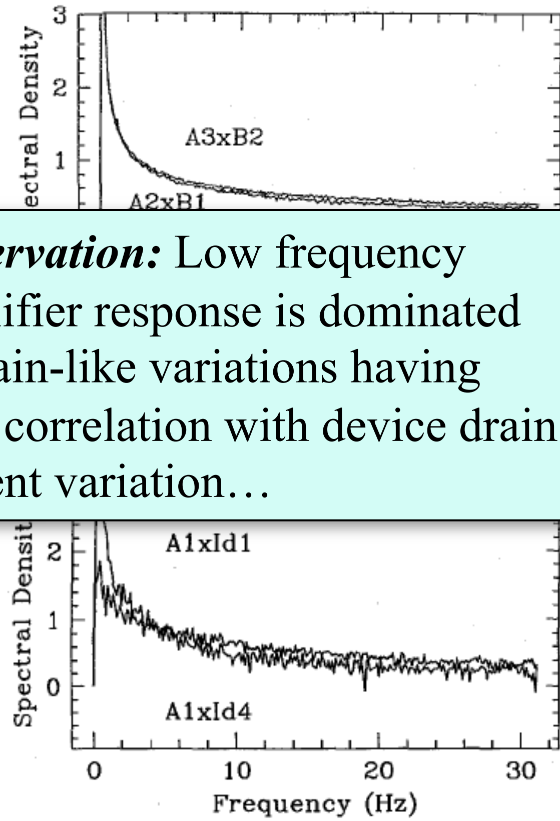

Observation: Low frequency amplifier response is dominated by gain-like variations having ~0.3 correlation with device drain current variation…

Fig. 9. Cross-correlations between the output power of radiometer chan
$A1$ and the drain current of the input transistor of the HEMT amplif
$(A1 \times I_{d1})$ and the drain current of the final transistor of the HEMT amplif
$(A1 \times I_{d4})$.

$$\rho_{\delta g\, i_d} = \left. \frac{\langle \delta g \cdot \delta i_d \rangle}{\sqrt{\langle \delta g^2 \rangle \langle \delta i_d{}^2 \rangle}} \right| \sim 0.3$$

Jarosik, N. "Measurements of the low-frequency-gain
cryogenic amplifier", 1996, IEEE Transactions on Mic

Stabilization Spin-Off Ideas…

- Stabilization or "Pilot" Tone…
- Multi-Level Calibration…
- Pre-Whiten Data to Limit Noise…
- Use Measurement Transconductance or Drain Current as Proxy for Gain Variation and Correct Radiometric Data…

…all of these approaches have limitations in addressing underlying concern for precision broadband radiometry…

Comments: If the device conductance is varying the associated capacitances (i.e., $C_{ds,}$ $C_{dg,}$ $C_{gs,\ldots}$) in the region will also change. This can be seen by considering the influence of variations in the local conductivity and dielectric constant (e.g., as initiated by interaction of charges with *g-r* trap site) on the device's model parameters. The parameter's mean and variance need to be consistently handled in modeling the response…

Device Scaling Perspective…

- HEMT Noise, Gain, and Stability are fundamentally linked:

$$T_{\min} \approx \sqrt{T_d T_g} \cdot \frac{f_{\max}}{f} \qquad G_{A_{opt}} \approx \sqrt{\frac{4T_d}{T_g} \cdot \frac{f_{\max}}{f}}$$

$$f_{\max} \sim f_T \approx \frac{v_{sat}}{2\pi l_g} \qquad \frac{\langle i_v^2 \rangle}{I^2} \sim \frac{\alpha_H}{N_c f}$$

$$S_T = T_{sys} \cdot \left[\frac{2}{\Delta v_{rf}} + \delta g^2(f) + \delta t^2(f) \right]^{1/2}$$

Gain variation increases as device gate scale reduced…

$$\delta t^2(f) \ll \delta g^2(f) \propto \frac{N_{stages}}{A_{gate} J_{ds}} \cdot \frac{1}{f}$$

Variation can yield inter-channel correlation…

$$\rho_{ij} = \left. \frac{\delta g^2(f)}{2/\Delta v_{rf} + \delta g^2(f)} \right|_{\Delta v_{rf} = 1GHz, f = 10\,Hz} \sim 0.3$$

Wollack, E.J., "High-Electron-Mobility-Transistor Gain Stability and its Design Implications for Wide Band Millimeter Wave Receivers," 1995, Review of Scientific Instruments, Vol. 66(8), pp. 4305-4312.

WMAP: A Case Study...

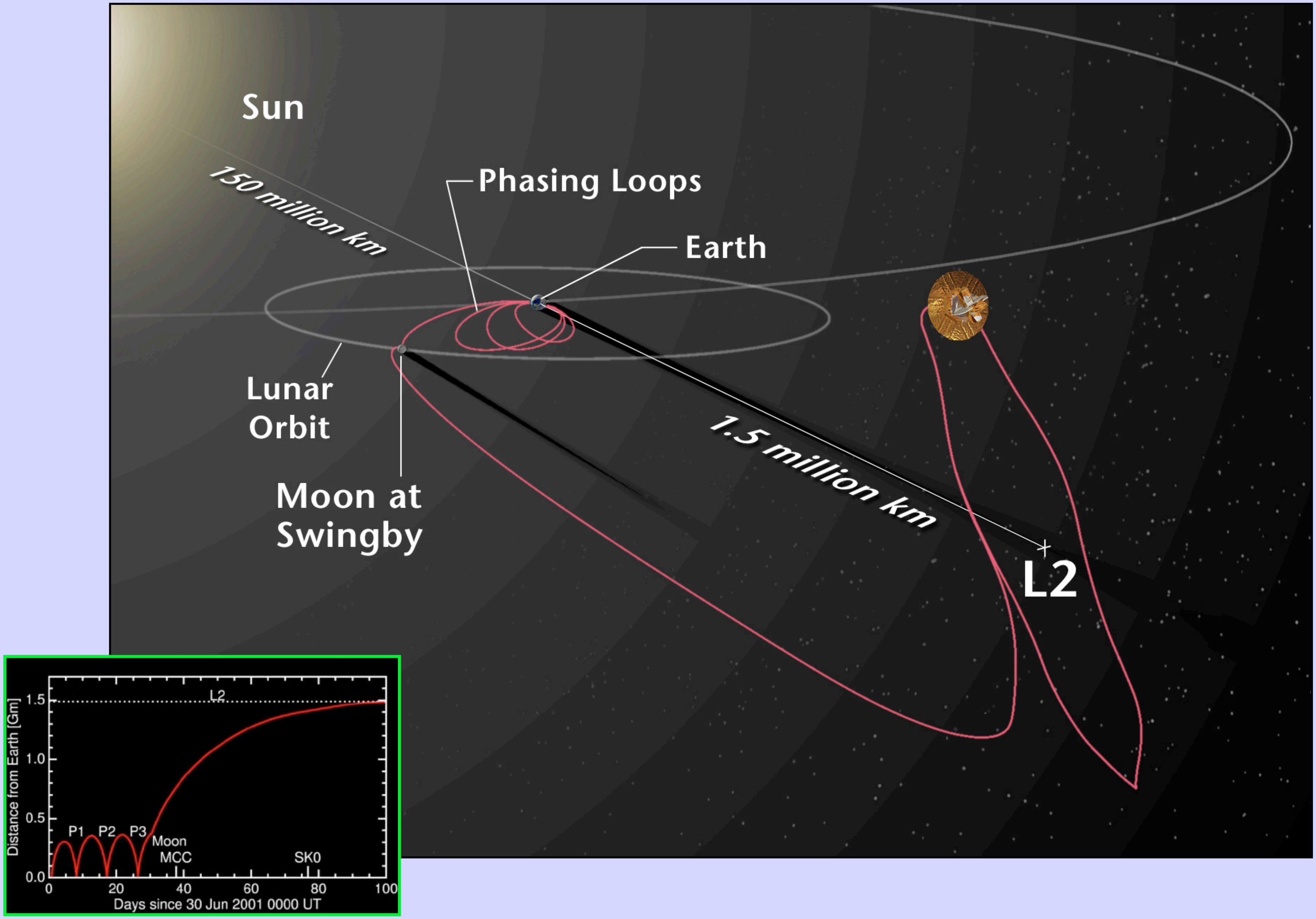

WMAP: Experimental Approach

- Differential radiometer design to minimize systematic errors
- 5 microwave frequencies to understand foregrounds
- 20 radiometers to allow multiple cross checks
- Sensitivity to polarization
- Accurate calibration (<0.5%)

  → in-flight calibration using modulation of the dipole
- In-flight beam measurements on Jupiter
- Minimize sidelobes & diffracted signals from Earth, Sun, Moon
  → L2 orbit
- Multiple modulation periods to identify systematic effects
- Minimize all observatory changes

  → L2 orbit; constant survey mode operations
- Thermal stability / Passive thermal control → L2
- Rapid and complex sky scan

  →observe 30% of the sky in an hour

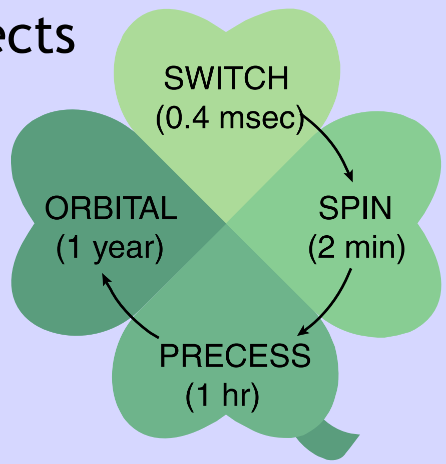

SPIN-SYNCHRONOUS NON-SKY SIGNALS WERE THE LEADING CONCERN

WMAP Scan Strategy

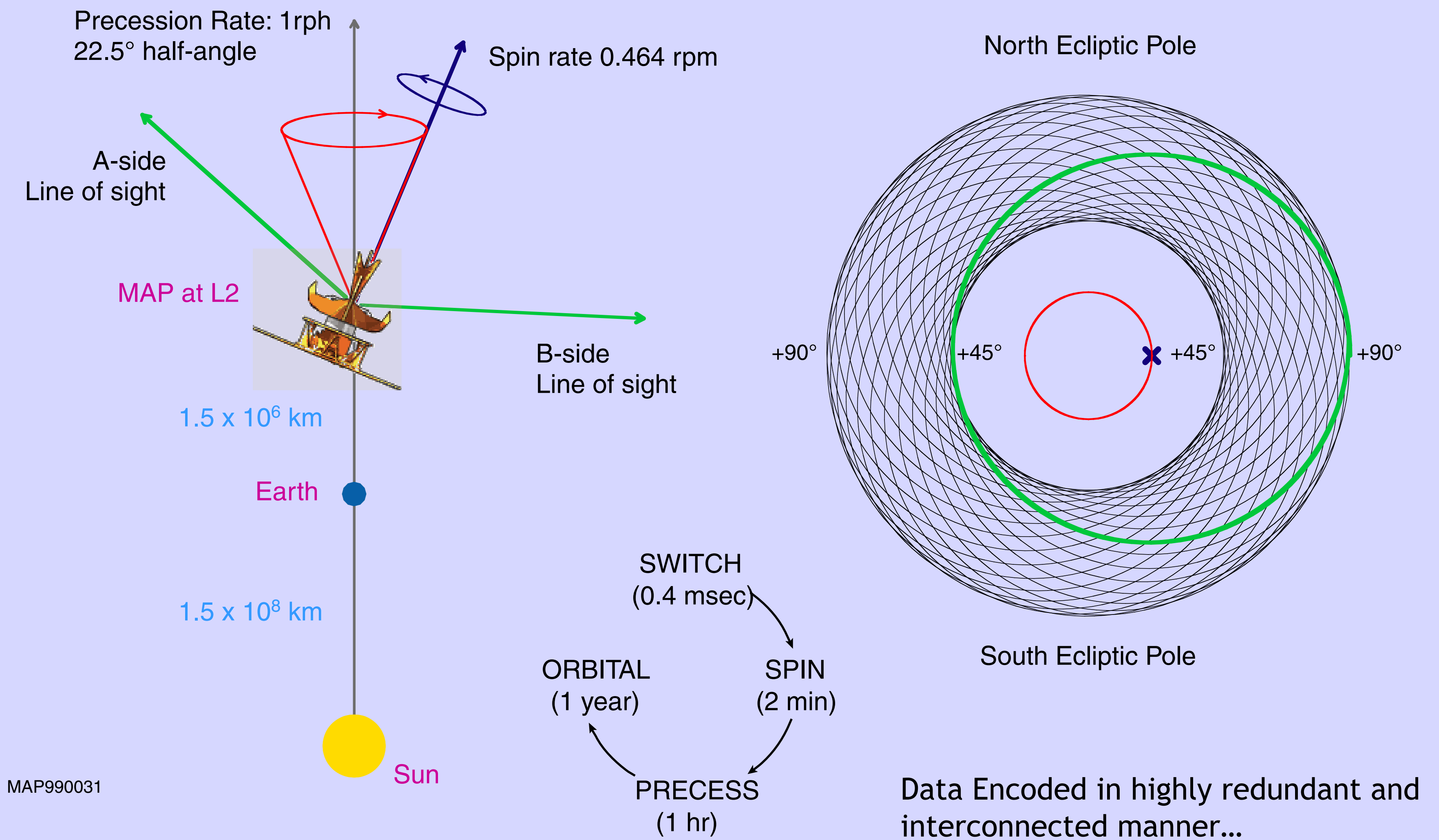

Data Encoded in highly redundant and interconnected manner…

WMAP: HEMT-Based Differential Receivers

10 "Differencing Assemblies"

4 @ 94 GHz W-band
2 @ 61 GHz V-band
2 @ 41 GHz Q-band
1 @ 33 GHz Ka-band
1 @ 23 GHz K-band

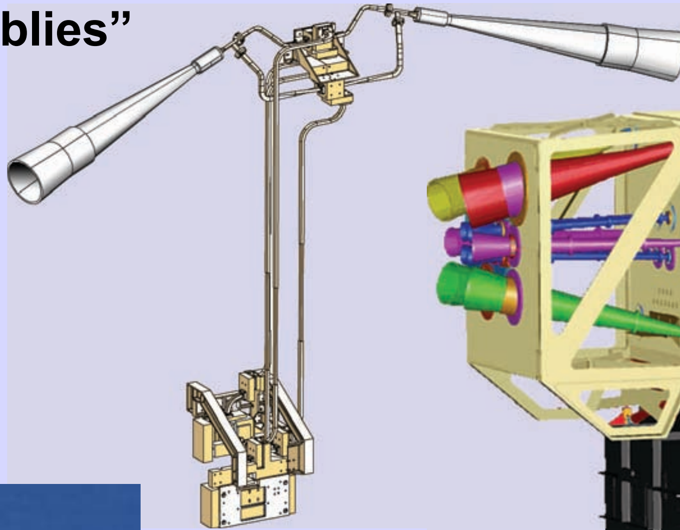

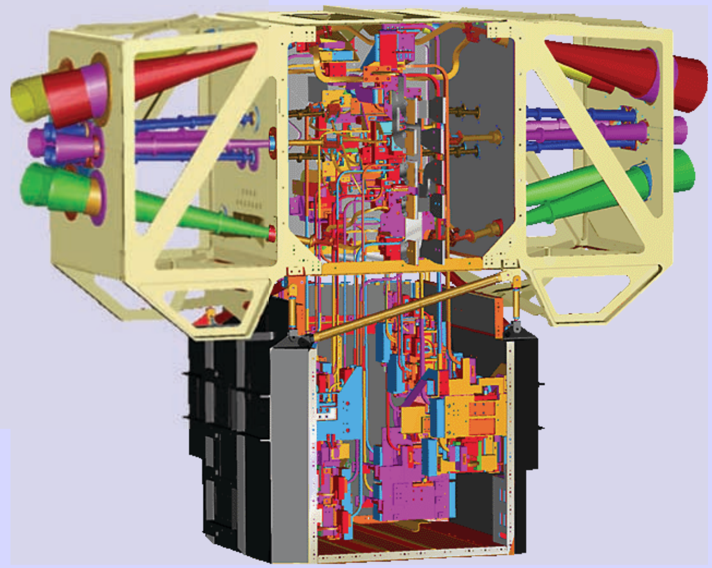

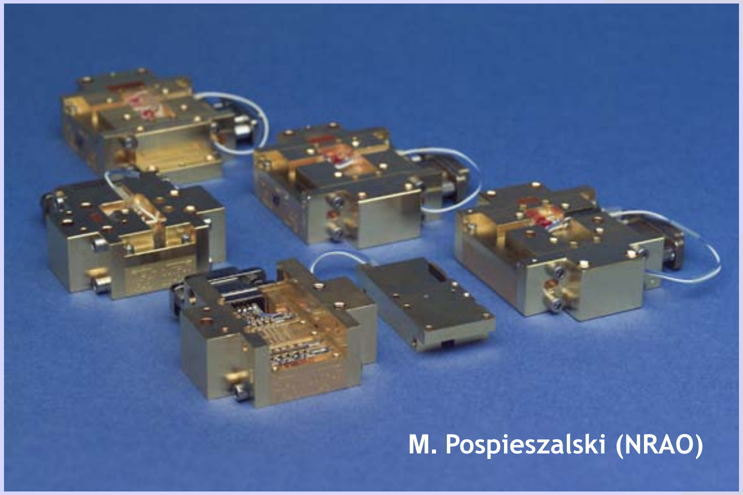

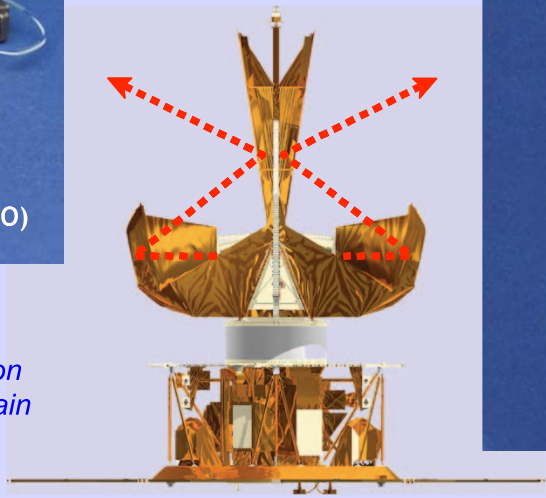

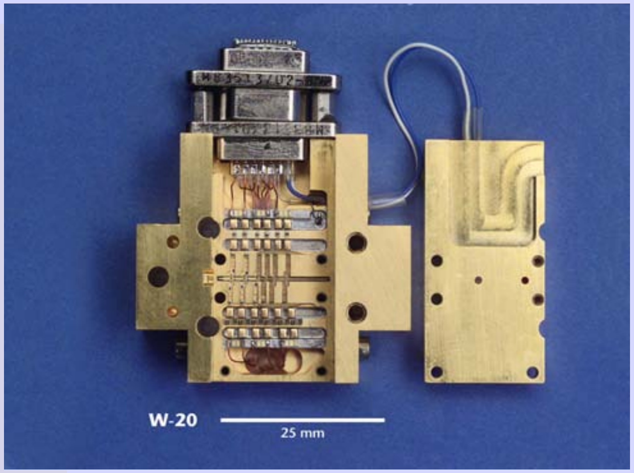

WMAP'S Purpose…

To make a detailed full-sky map of the CMB radiation anisotropy (temperature and polarization) to constrain the cosmology of the universe…

WMAP: Pseudo-Correlation Radiometer

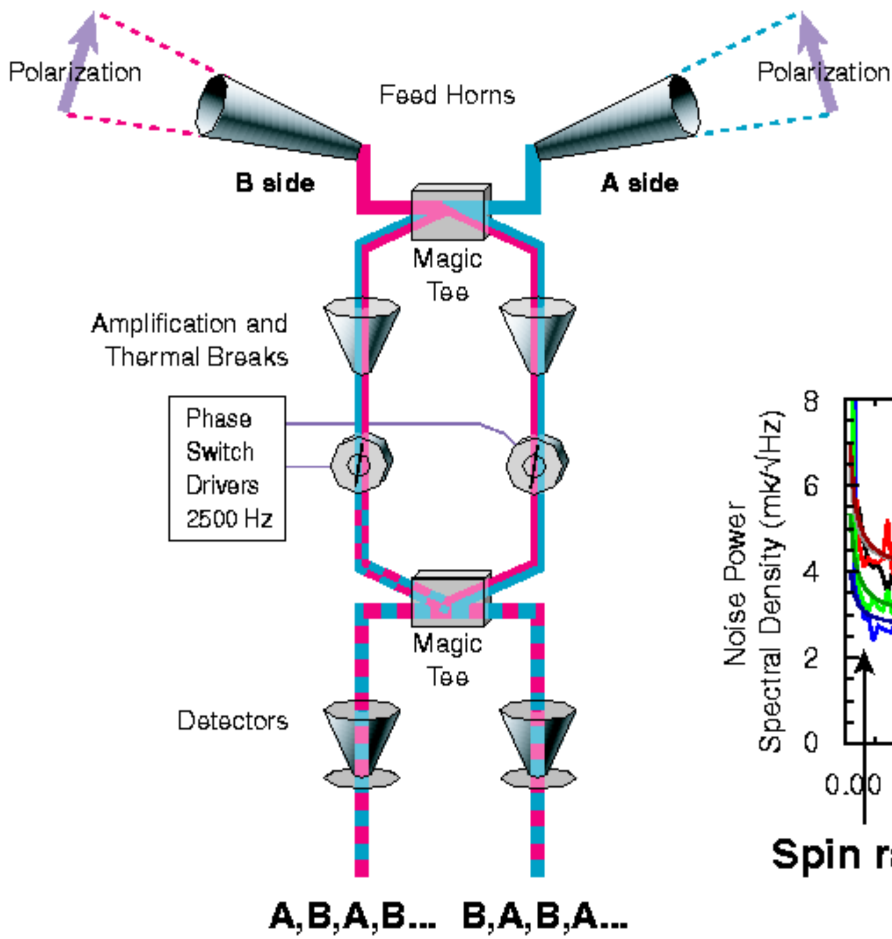

Why no *1/f* noise?

- Rapid switching at 2500 Hz chops faster than gain variations…

- Gain fluctuations are common to A and B and cancel upon differencing.

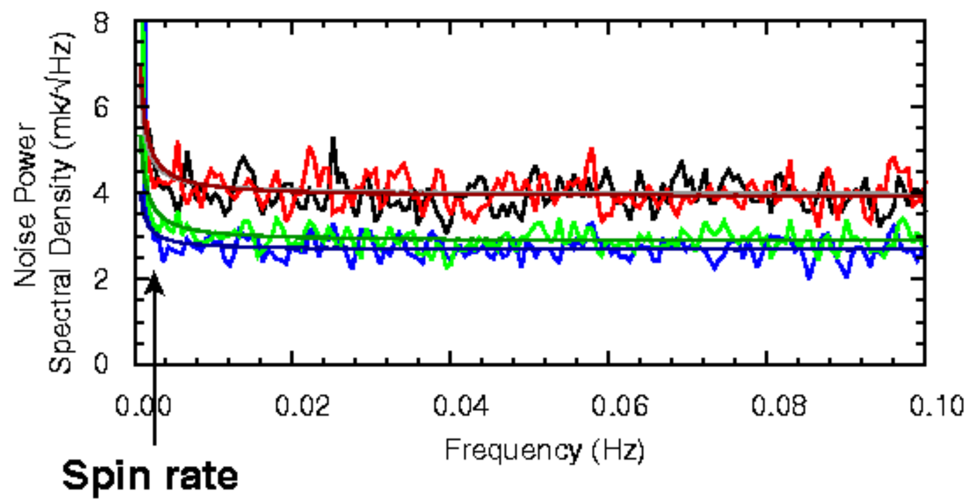

WMAP: Pseudo-Correlation Radiometer

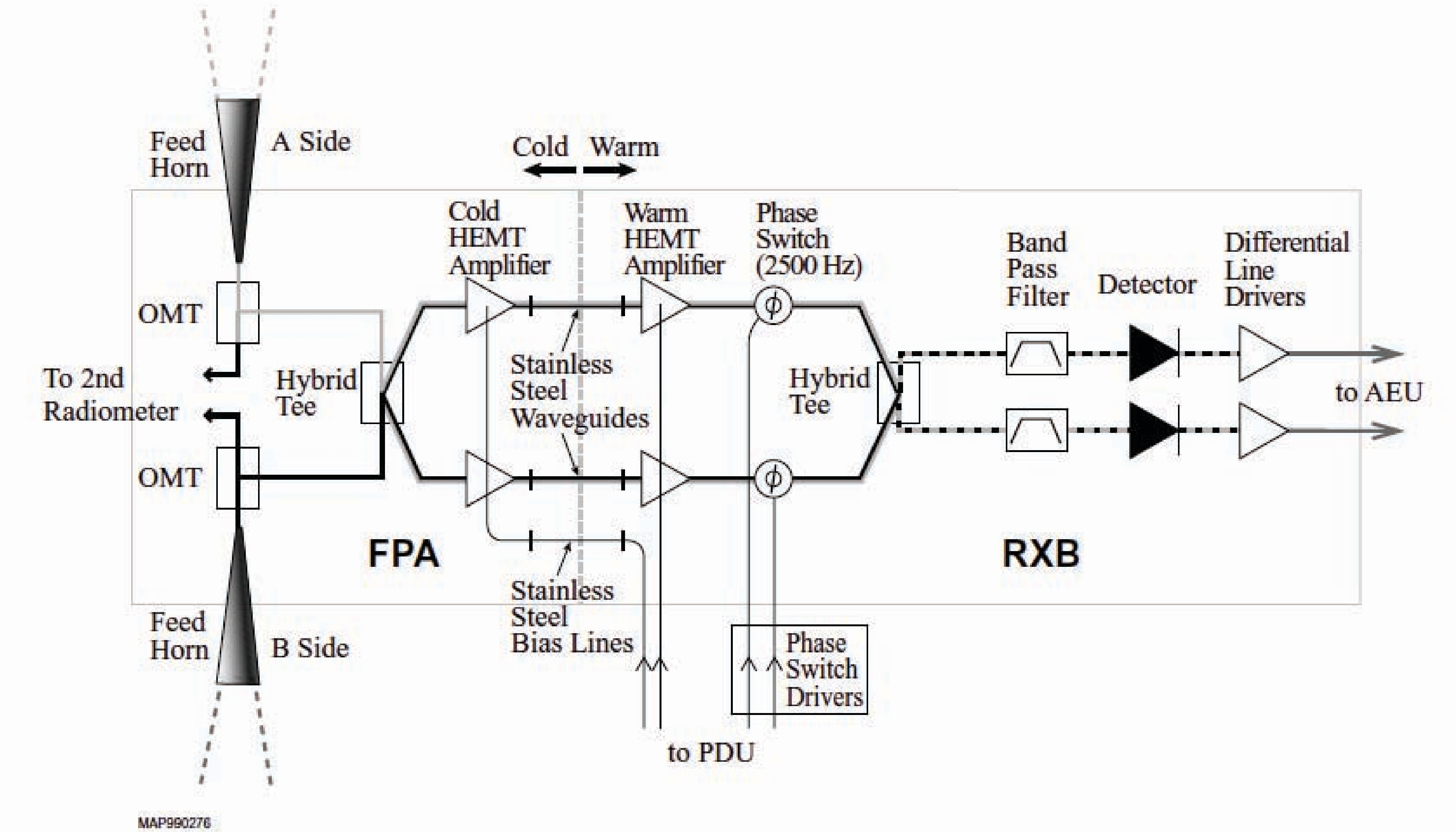

Jarosik, N., et al., "Design, Implementation, and Testing of the Microwave Anisotropy Probe MAP Radiometer", ApJS 145:413–436, 2003

WMAP: W-Band Amplifier

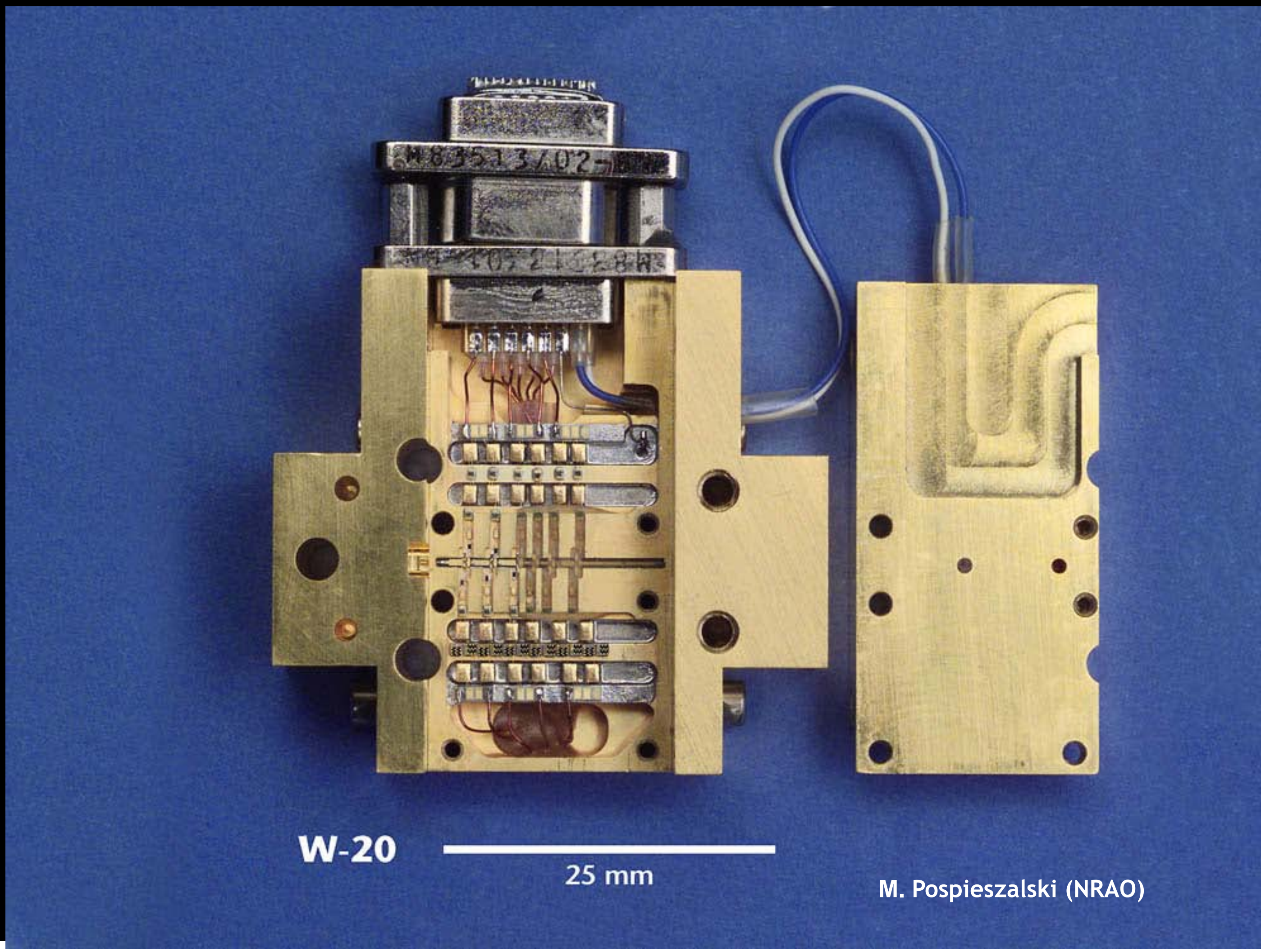

NRAO: Noise/Gain Measurement Dewar

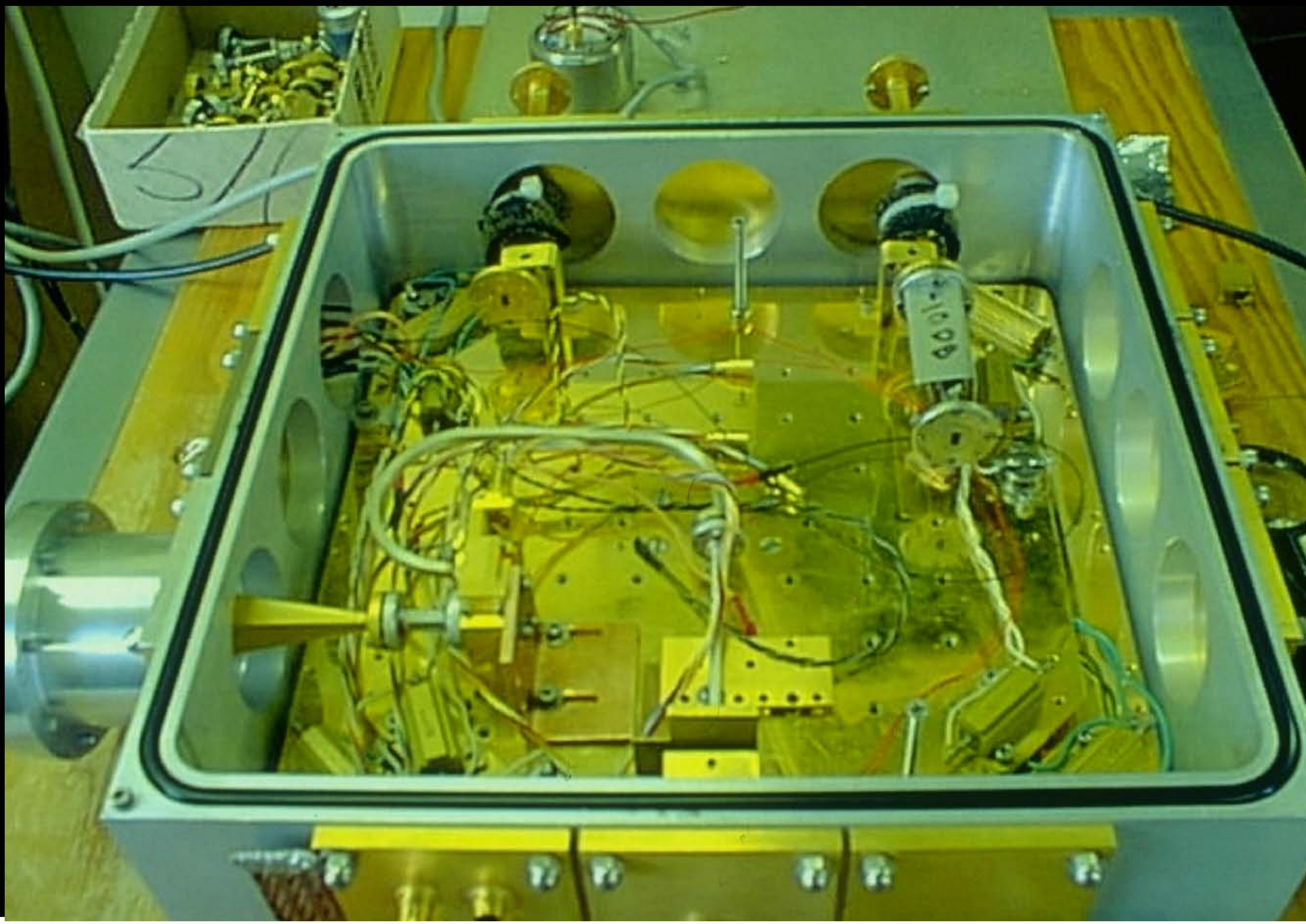

WMAP: W-Band Amplifier Gain

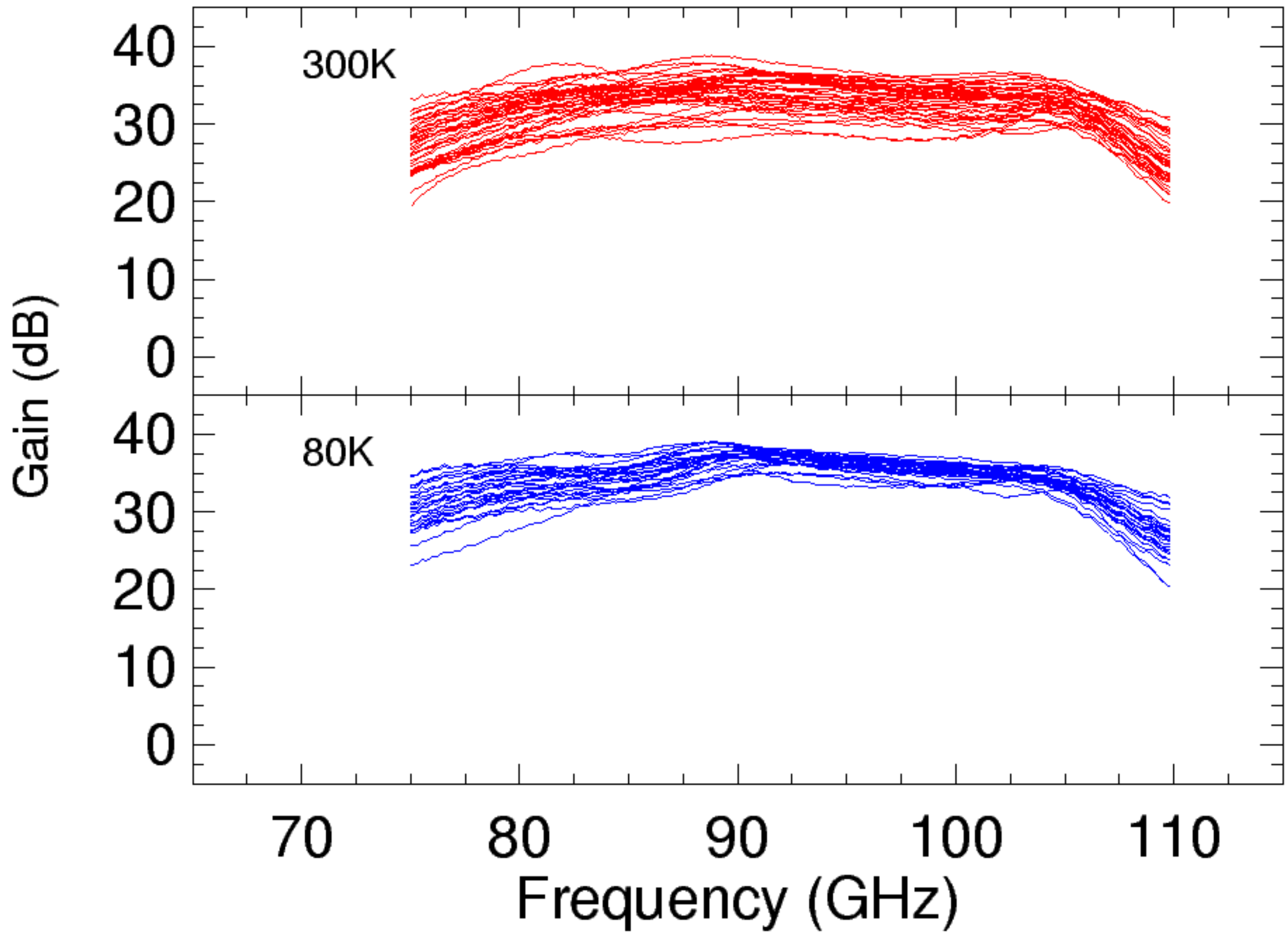

Pospieszalski, M.W., et al., “Design and Performance of Wideband, Low-Noise, Millimeter-Wave Amplifiers for Microwave Anisotropy Probe Radiometers,” 2000, IEEE MTT-S International Microwave Symposium Digest, Boston, MA, pp. 25-28.

WMAP: W-Band Amplifier Phase Tracking

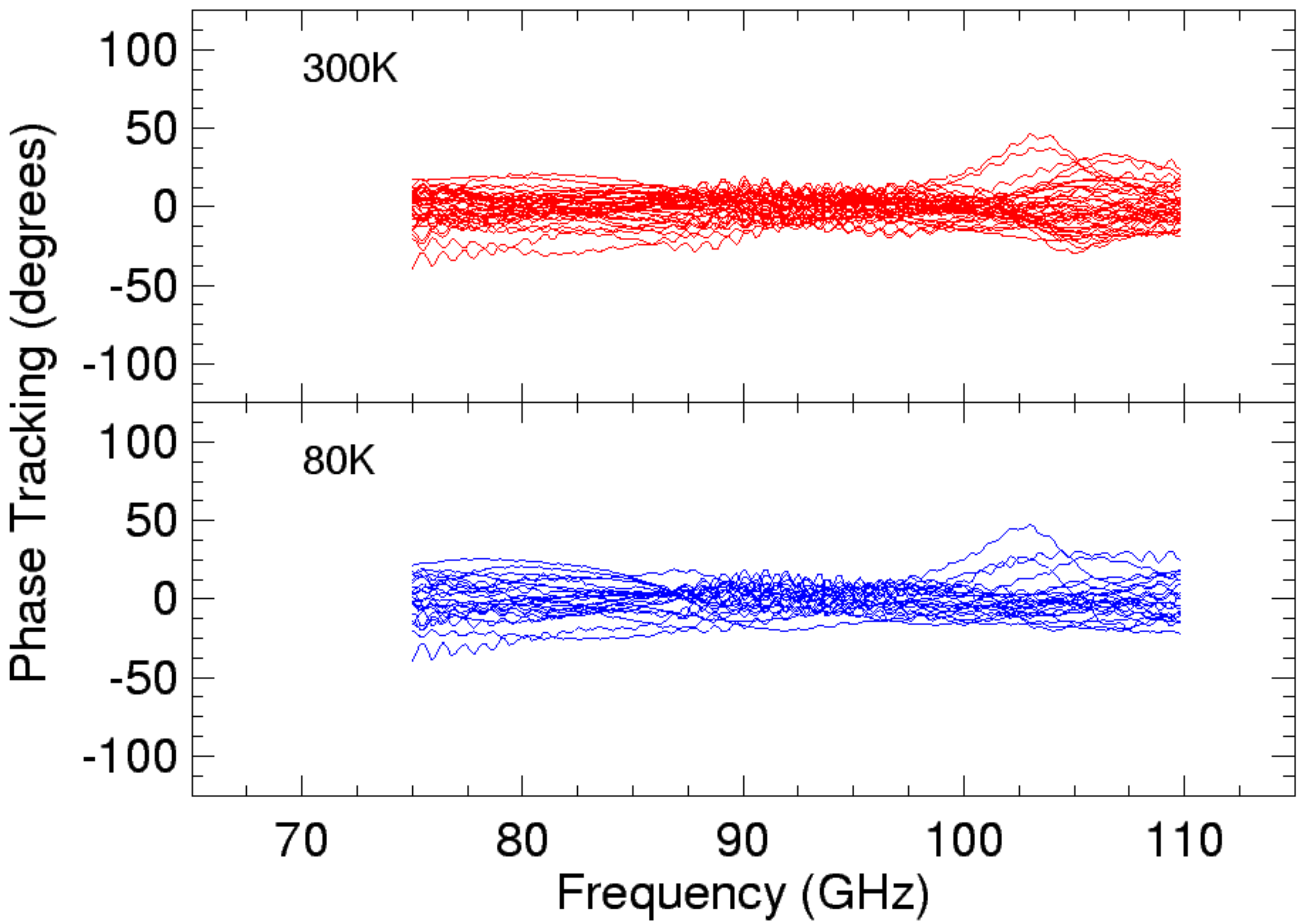

WMAP: Amplifier Noise Temperature

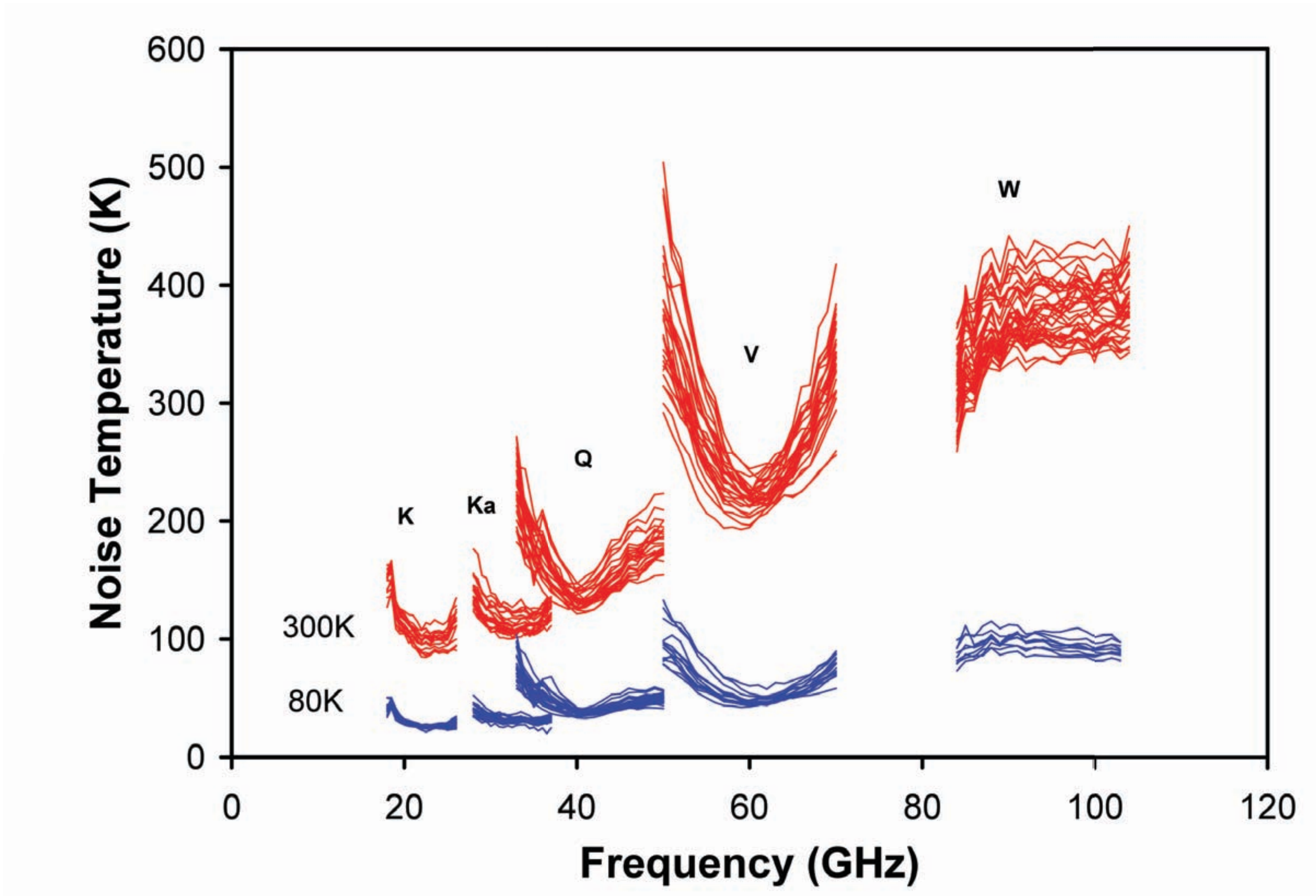

NRAO: Low Frequency Stability Test

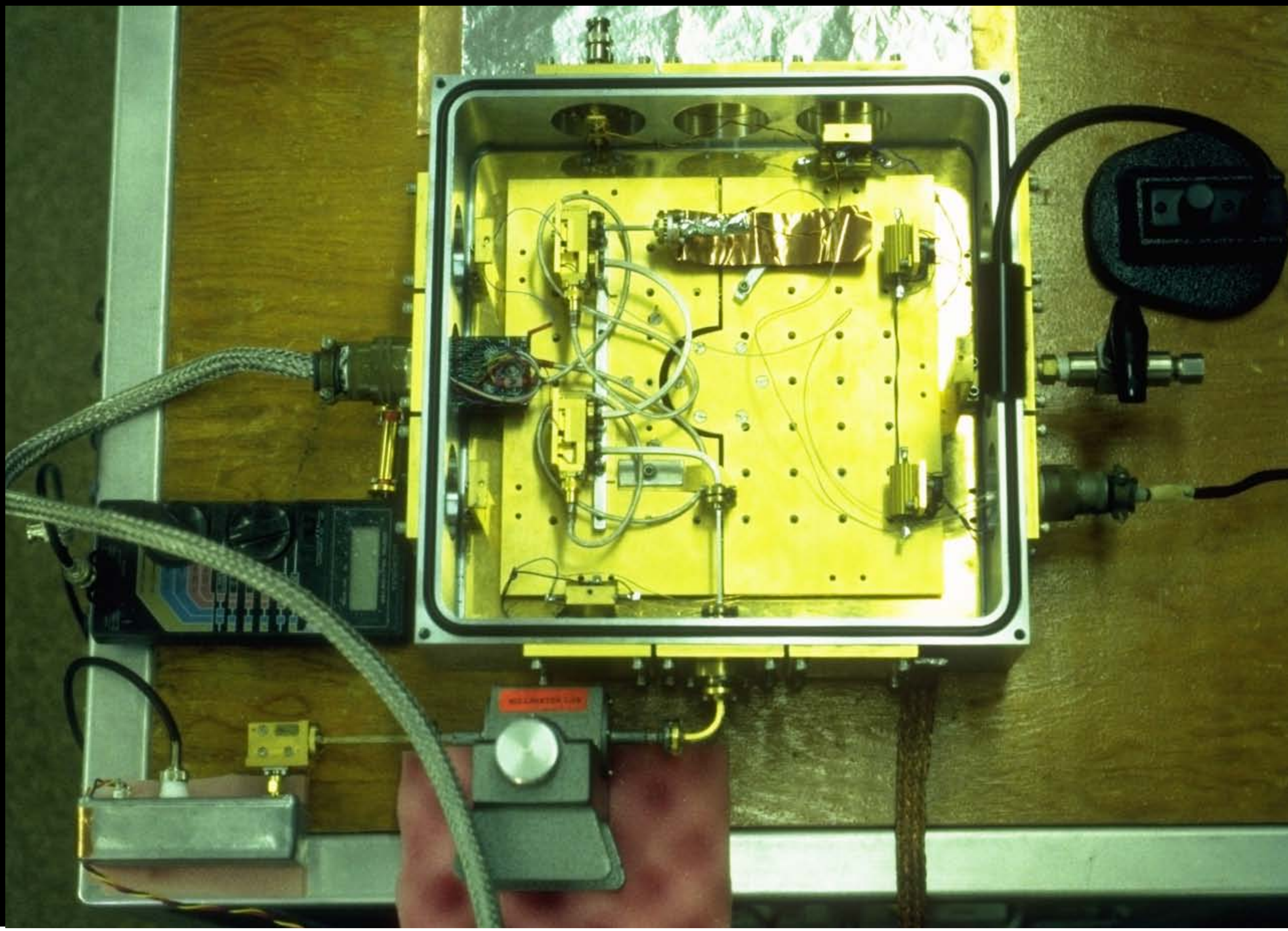

WMAP: Amplifier Stability Test and Scaling

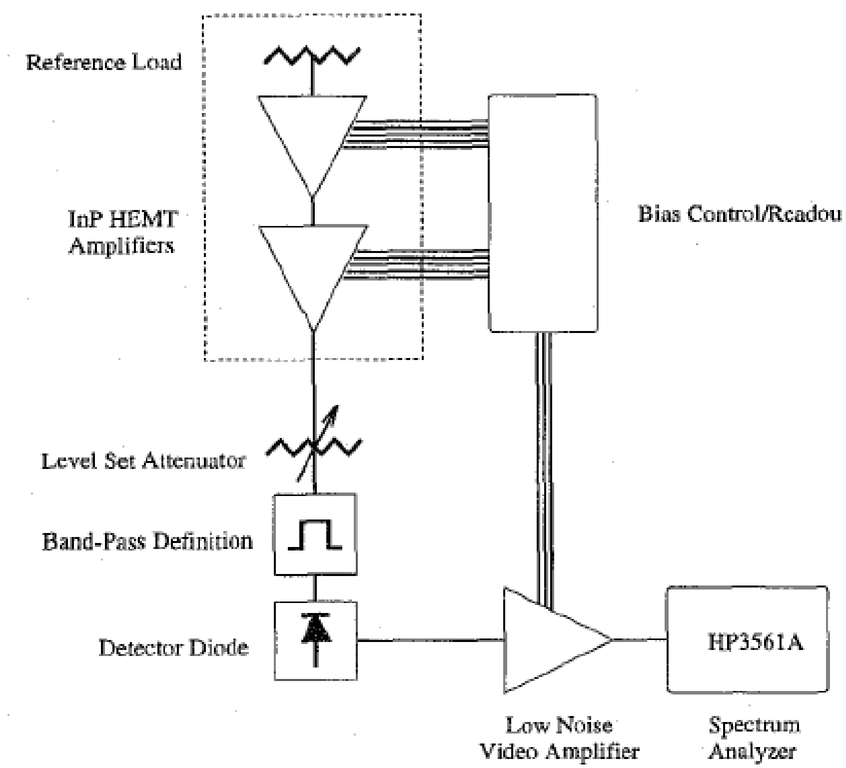

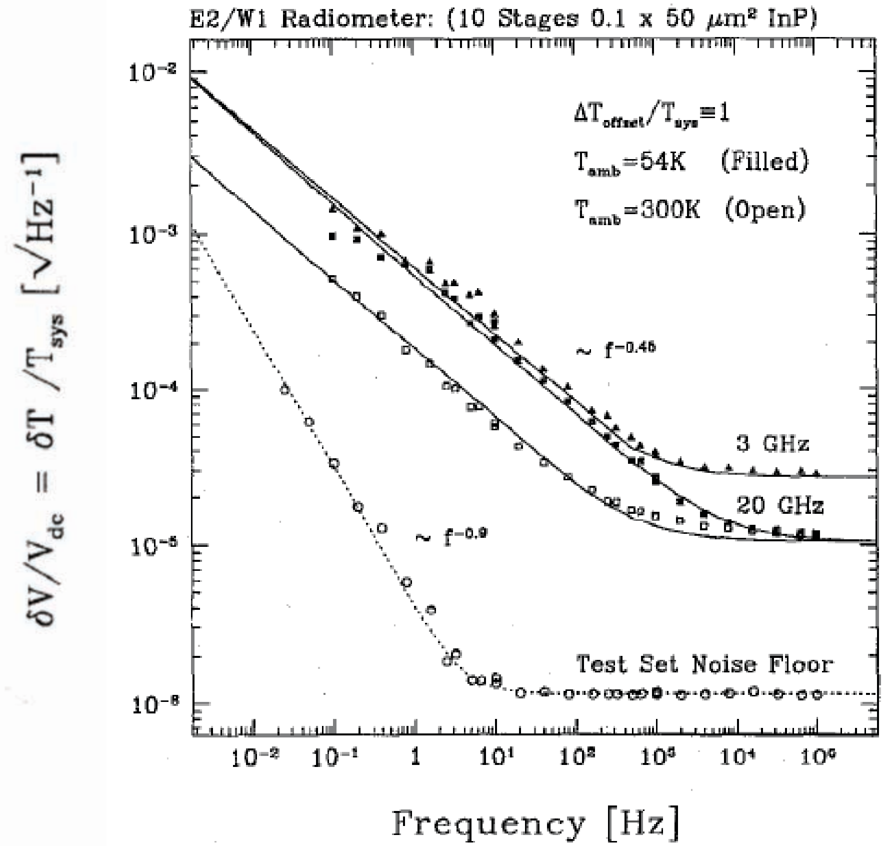

$$\frac{\delta V}{V_{\mathrm{dc}}} = \frac{\delta T}{T_{\mathrm{sys}}} = \kappa_o \left(\frac{2}{\Delta\nu_{\mathrm{rf}}} + \left(\frac{\Delta T_{\mathrm{offset}}}{T_{\mathrm{sys}}} \right)^2 \delta g^2(f) \right)^{1/2}$$

Observation: Receiver '*1/f*' knee frequency is a function of the spectral density of gain fluctuations, RF detection bandwidth, system noise, and radiometric offset – it is not a device invariant parameter…

Wollack, E.J. and Pospieszalski, M.W., "Characteristics of Broad-Band InP Millimeter-Wave Amplifiers for Radiometry," 1998, IEEE MTT-S International Microwave Symposium Digest, Baltimore, MD, pp. 669-672.

WMAP: Amplifier Stability Test and Scaling

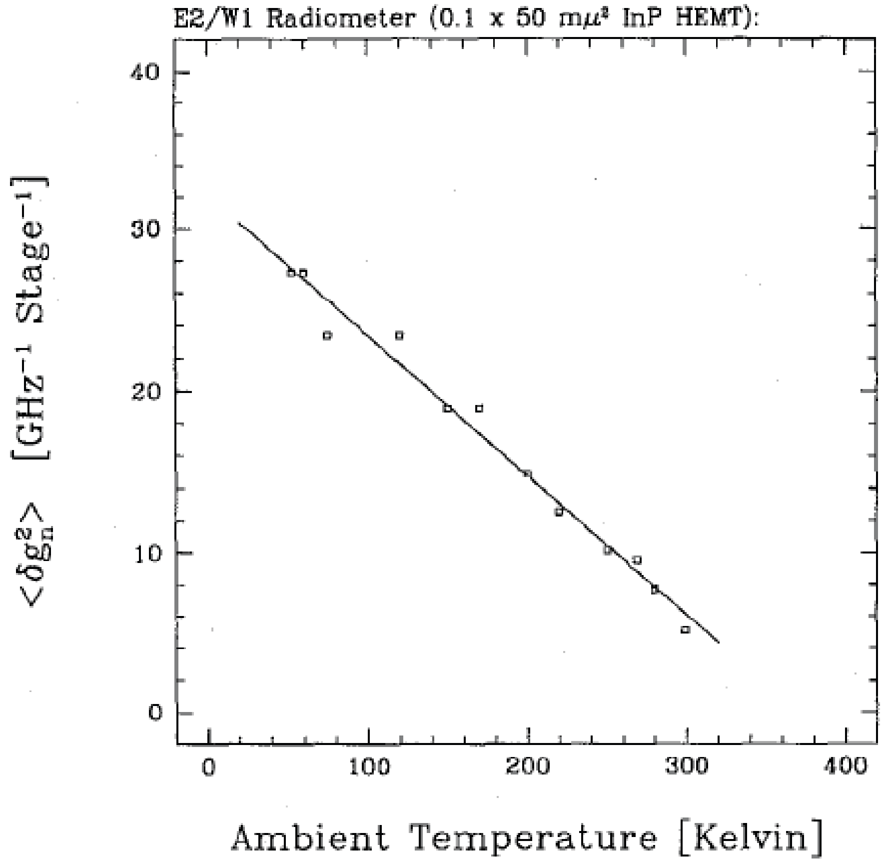

$$\frac{\delta V}{V_{dc}} = \frac{\delta T}{T_{sys}} = \kappa_o \left(\frac{2}{\Delta\nu_{rf}} + \left(\frac{\Delta T_{offset}}{T_{sys}} \right)^2 \delta g^2(f) \right)^{1/2}$$

Conclusion: Minimize total number of (cold) stages and radiometric offset…

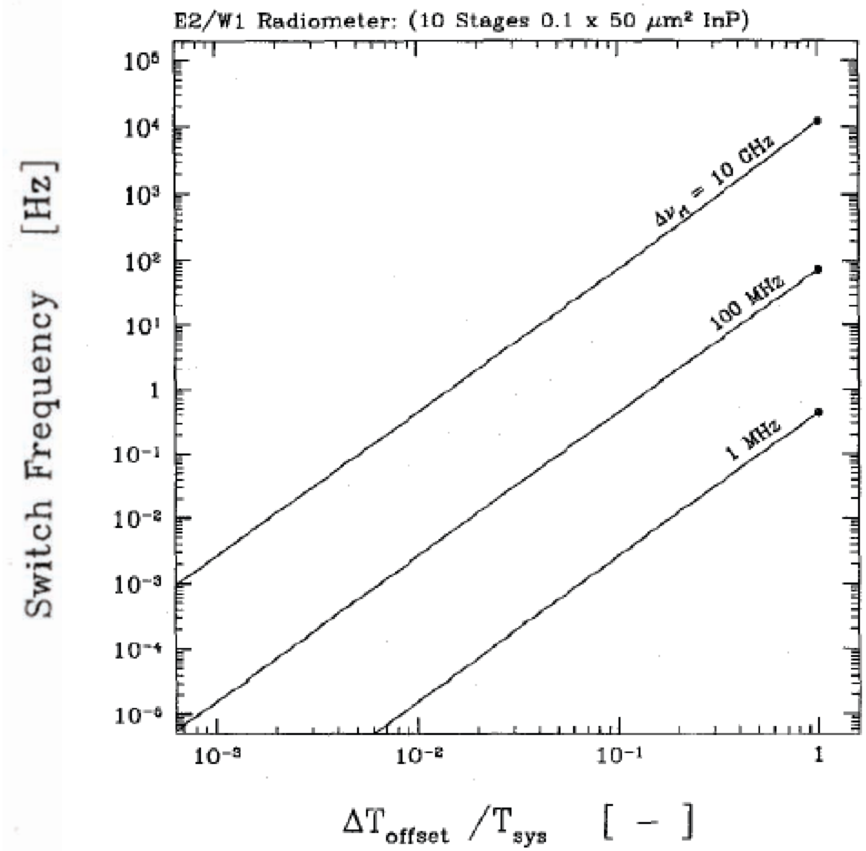

Fig. 4. Required switch frequency as a function of radiometer offset. The measured spectral index and density of gain fluctuations are used to estimate the switching frequency required to limit the noise contribution due to variations in the radiometer gain to 10% of the system noise. The filled dots indicate the switch frequency for a differencing or subtraction-type radiometer. The solid lines indicate the calibration rate required in a correlation or multiplication-type receiver as a function of the deviation from a balanced output.

Interlude – A Tale of Two Receivers:

Instrument Architecture and Device Stability…

Beam Switched Total Power Receiver…

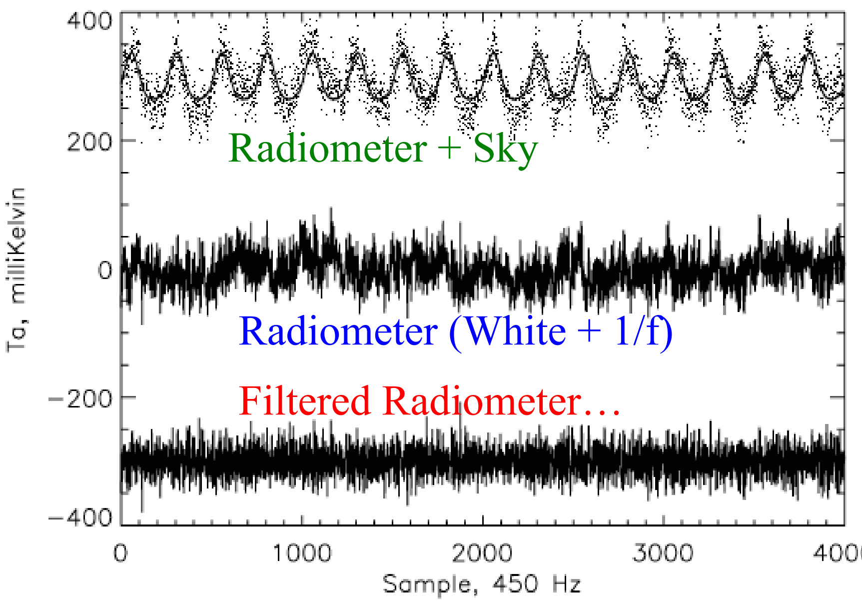

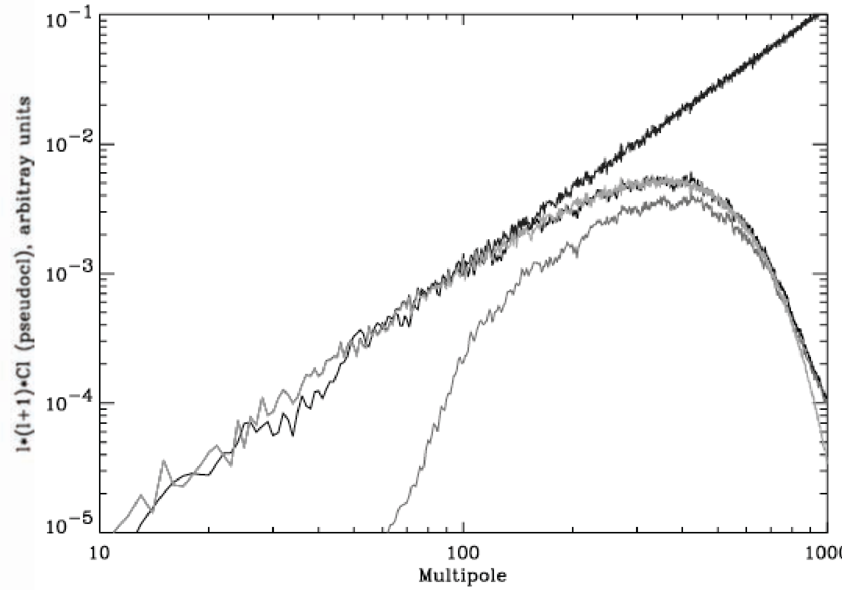

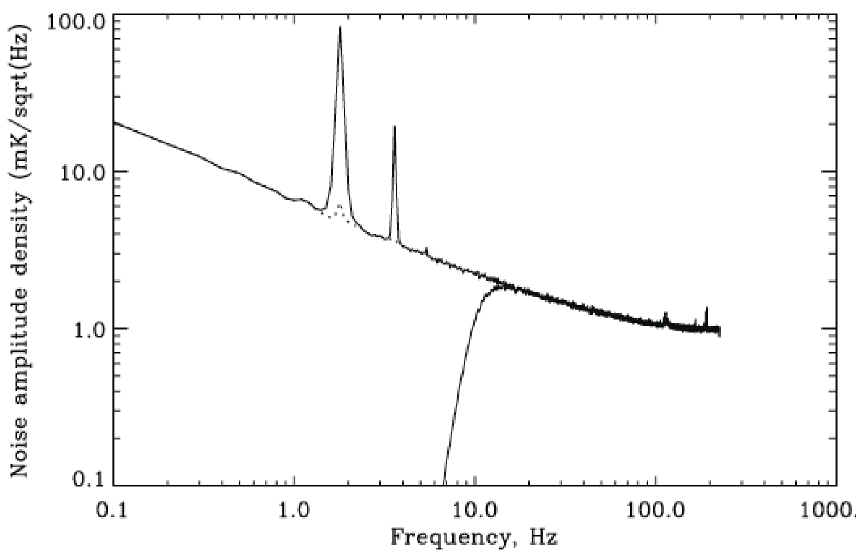

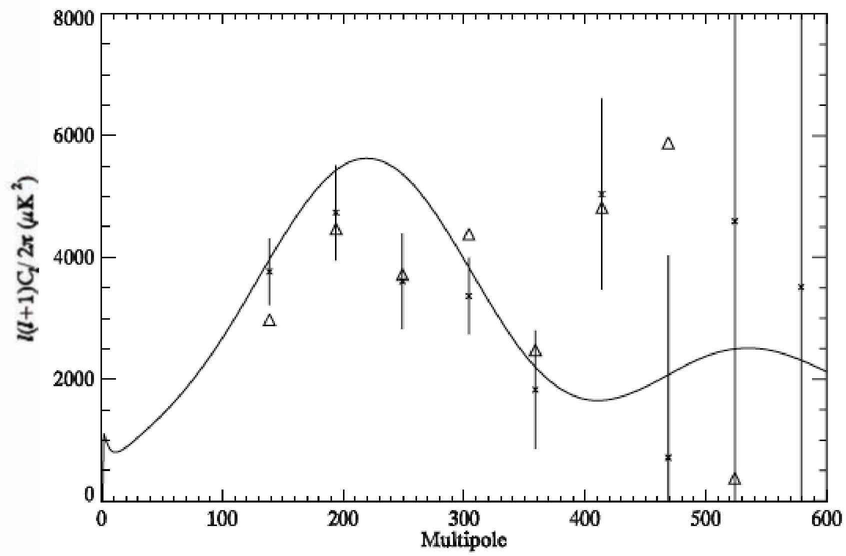

Interlude – A Tale of Two Receivers:

Instrument Architecture and Device Stability…

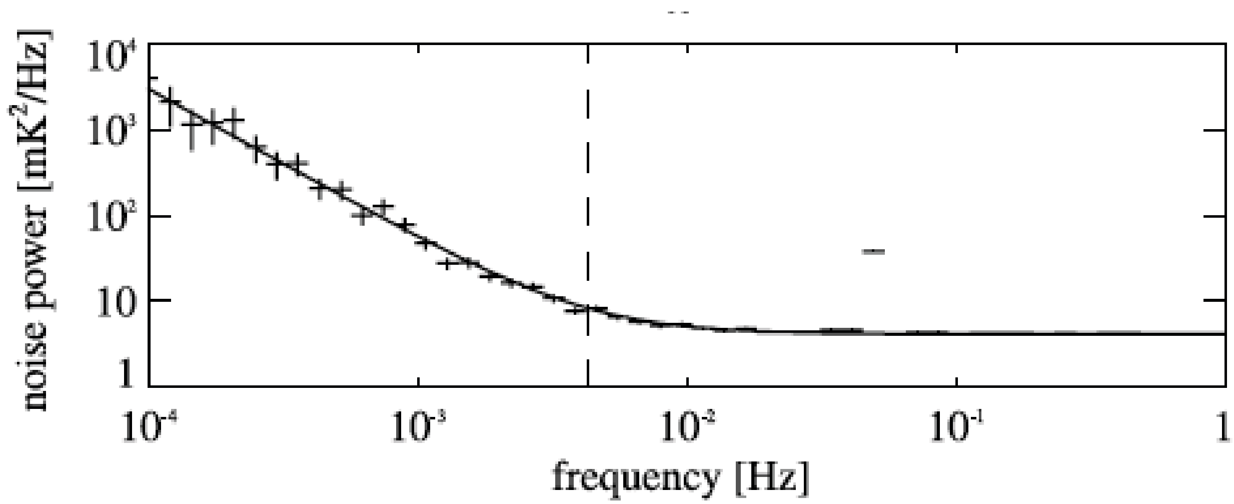

Bishop, C., et al., "New Measurements of Fine-Scale CMB Polarization Power Spectra from CAPMAP at both 40 and 90 GHz", ApJ 684:771Y789, 2008

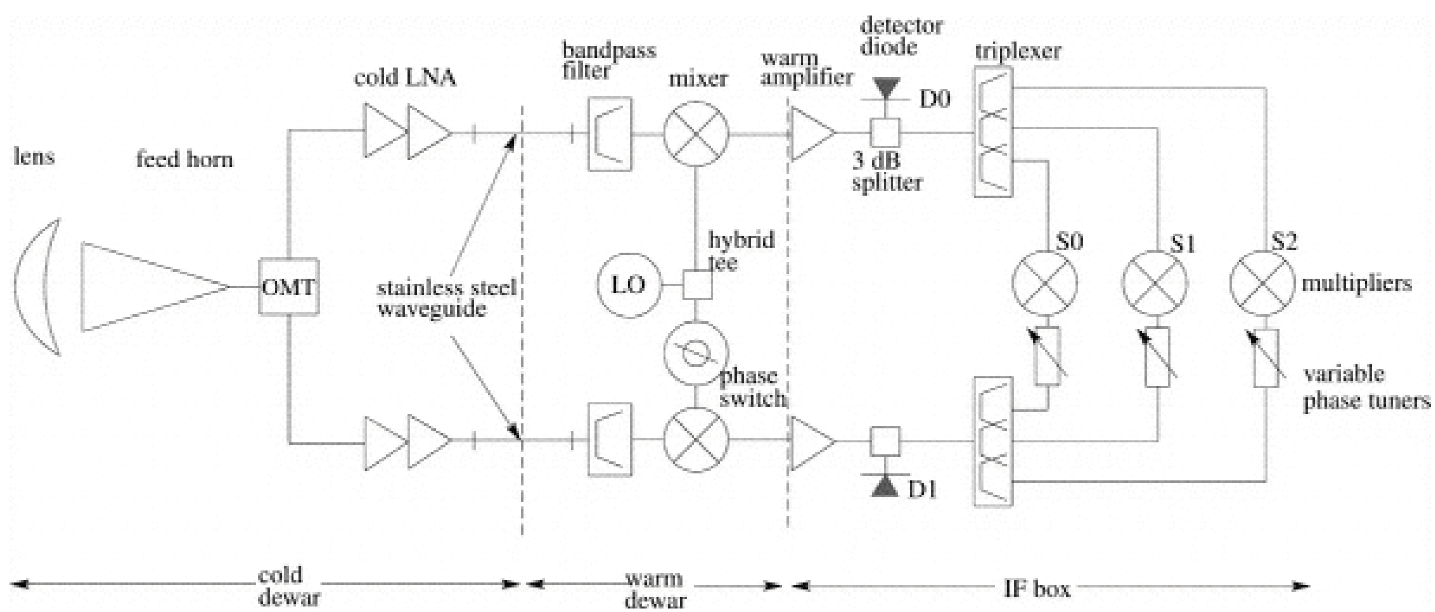

Barkats, D., et al., "Cosmic Microwave Background Polarimetry Using Correlation Receivers with the PIQUE and CAPMAP Experiments", ApJS 159:1-26, 2005

Heterodyne Correlation Polarimeter…

WMAP: Instrument Integration and Test

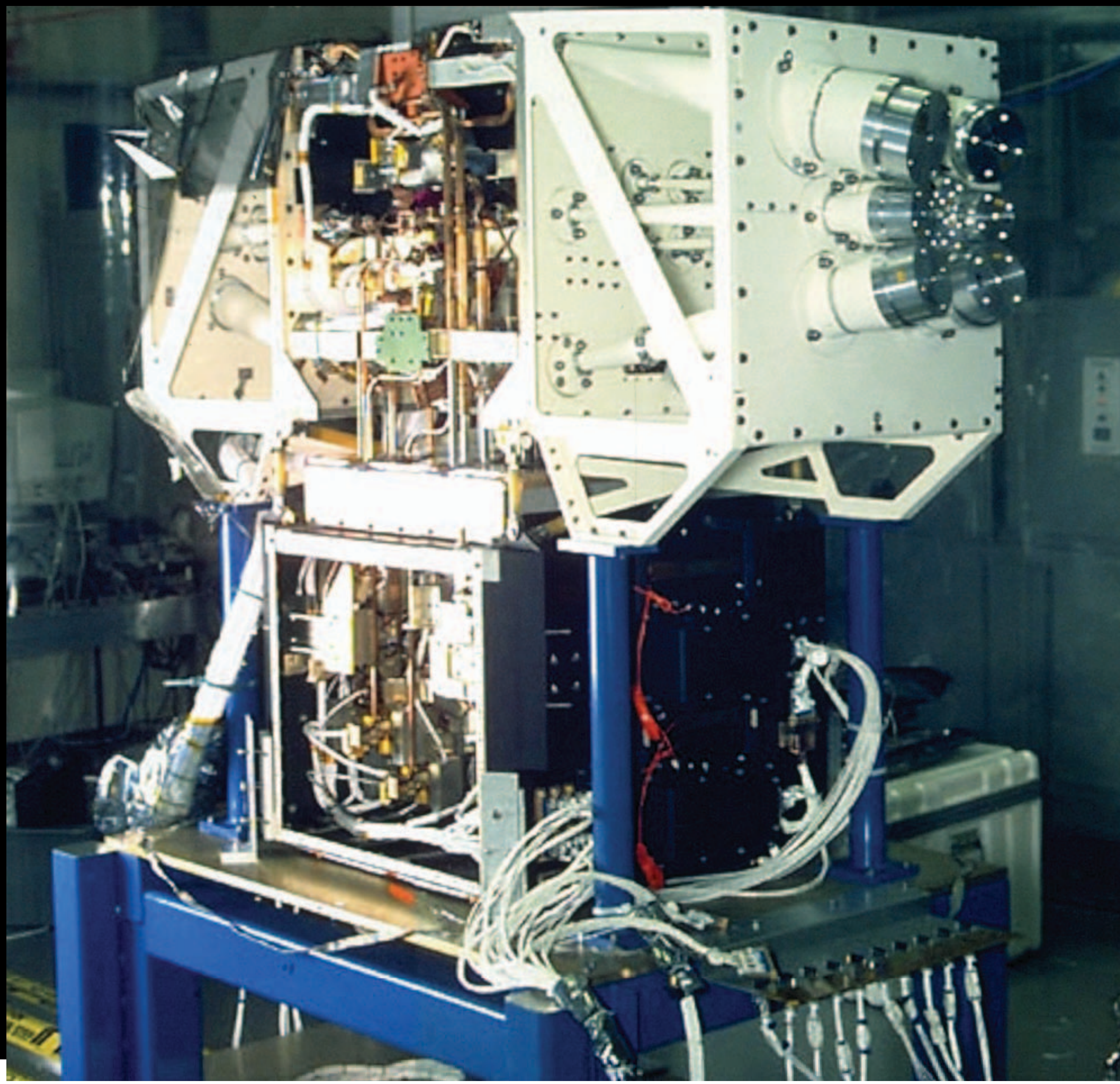

WMAP: Amplifier Life Test and Burn-In

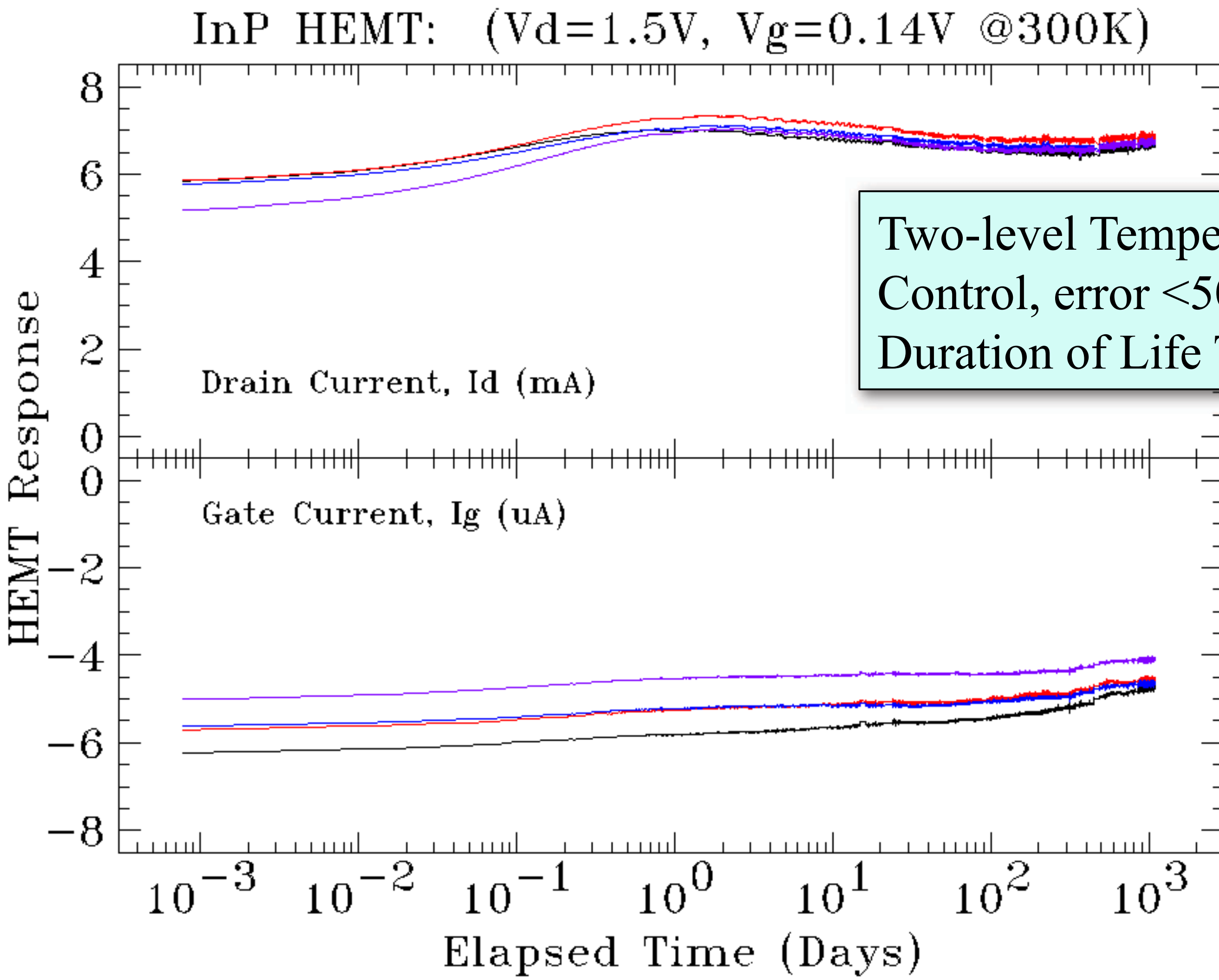

Two-level Temperature Control, error <50mK over Duration of Life Test…

Limon, M., et al., "Seven-Year Wilkinson Microwave Anisotropy Probe (WMAP) Observations: Explanatory Supplement," 2010, Version 4.0, http://lambda.gsfc.nasa.gov, pp. 1-190.

WMAP: Amplifier Life Test and Burn-In

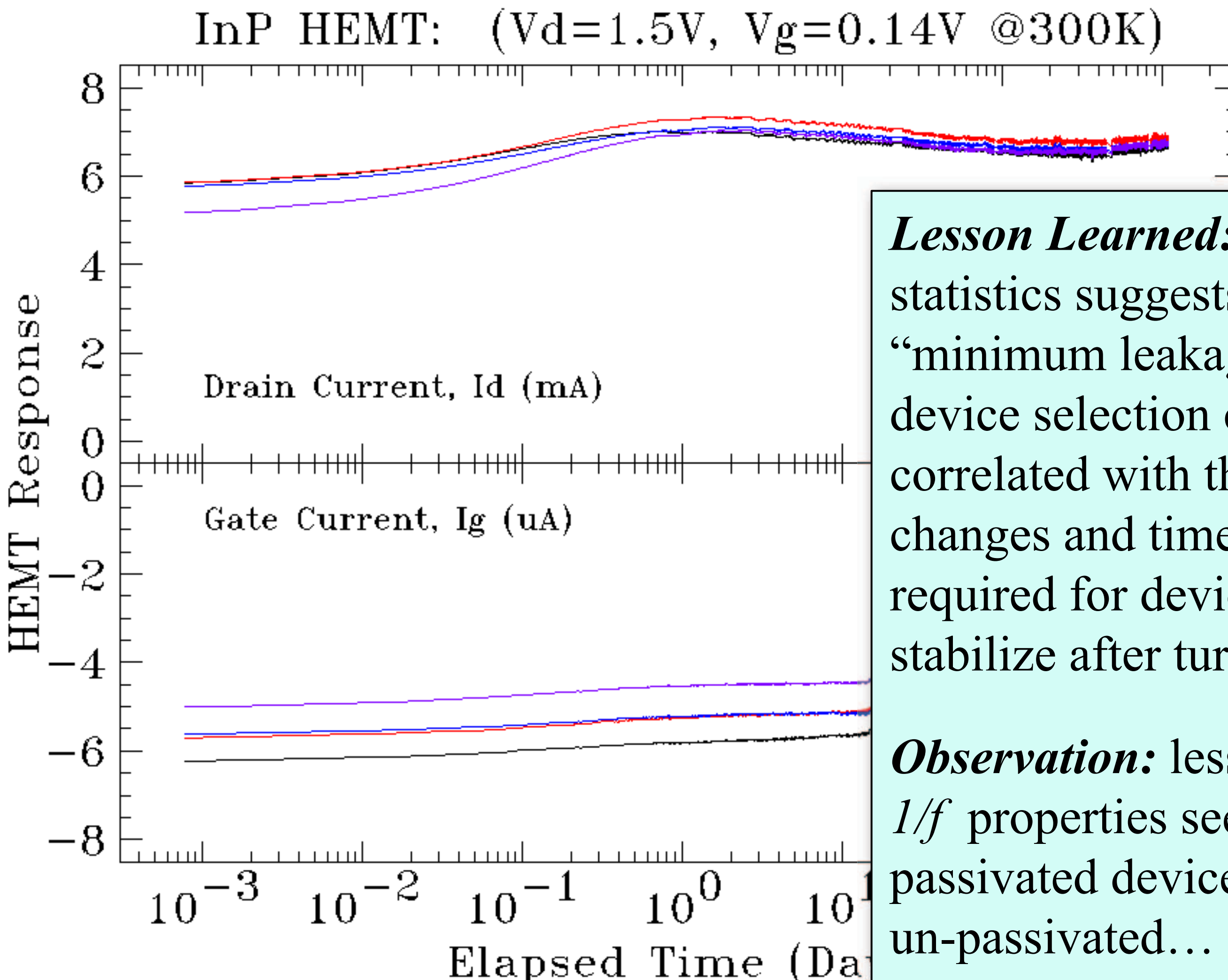

Lesson Learned: Build statistics suggests that the "minimum leakage current" device selection criteria is correlated with the observed changes and timescales required for device to stabilize after turn on…

Observation: less spread in *1/f* properties seen in passivated devices than in un-passivated…

Limon, M., et al., "Seven-Year Wilkinson Microwave Anisotropy Probe (WMAP) Observations: Explanatory Supplement," 2010, Version 4.0, http://lambda.gsfc.nasa.gov, pp. 1-190.

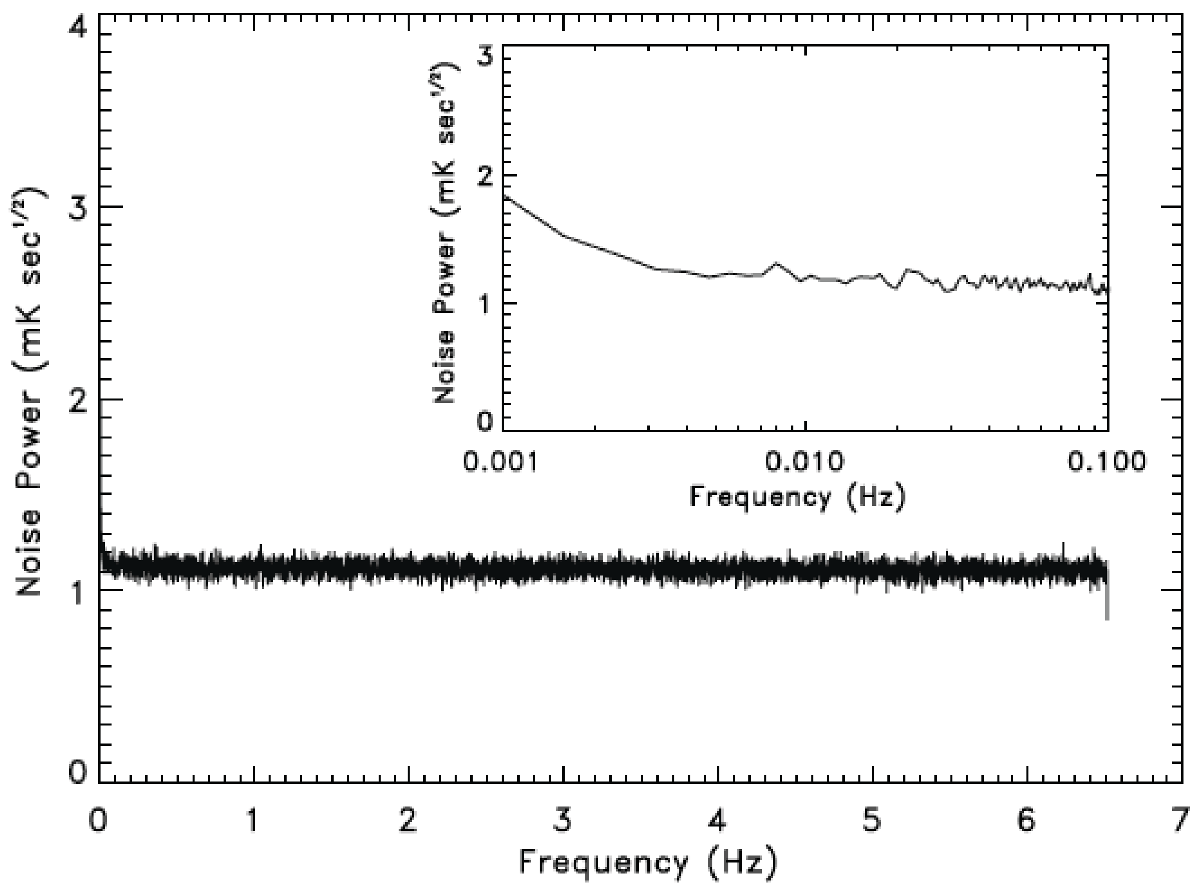

FIG. 2.—Noise power spectral density of the V12 radiometer obtained from 3 days of on-orbit data. Sky signals arising from the dipole, CMB, Galaxy, and point sources have been removed. The inset contains an expanded view of the low-frequency region of the same data. The flat spectrum down to very low frequencies ($f_{\text{knee}} = 1.41$ mHz) indicates proper radiometer performance.

Jarosik, N., et al., "First Year Wilkinson Microwave Anisotropy Probe (WMAP), Observations On-Orbit Radiometer Characterization, ApJS 2003, 148, 29-37.

$$\frac{\delta V}{V_{\mathrm{dc}}} = \frac{\delta T}{T_{\mathrm{sys}}} = \kappa_o \left(\frac{2}{\Delta\nu_{\mathrm{rf}}} + \left(\frac{\Delta T_{\mathrm{offset}}}{T_{\mathrm{sys}}} \right)^2 \delta g^2(f) \right)^{1/2}$$

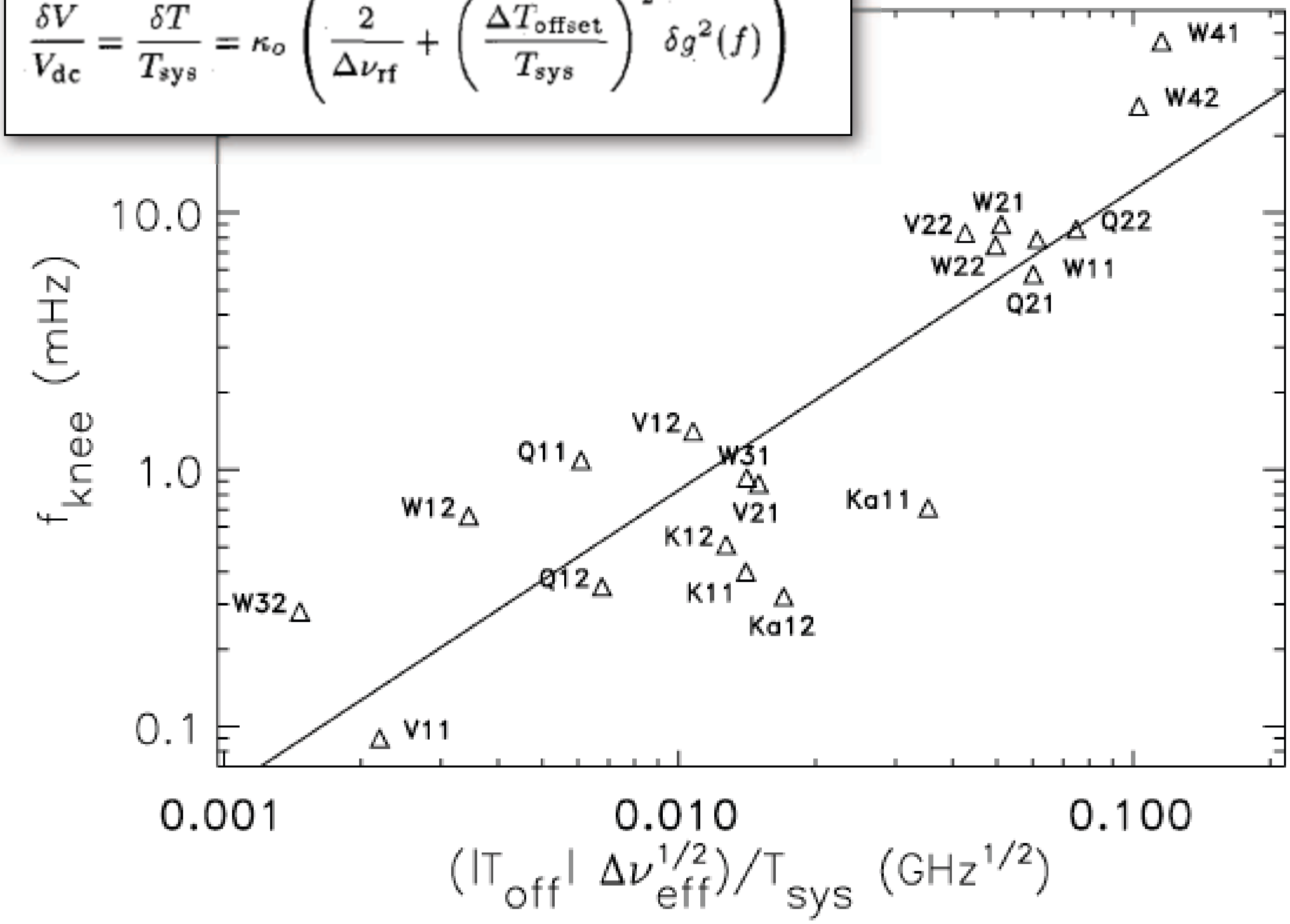

FIG. 3.—Dependence of f_{knee} on T_{off} for the 20 radiometers comprising *WMAP*. The solid line is a power-law fit to the data of the form $f_{\mathrm{knee}} \propto [(|T_{\mathrm{off}}|\Delta\nu_{\mathrm{eff}}^{1/2})/T_{\mathrm{sys}}]^{2/\alpha}$ with $\alpha = 1.70$. The scaling of f_{knee} with T_{off} indicates that f_{knee} is largely determined by radiometer gain fluctuations modulating the signal from the radiometer offsets, as expected.

Jarosik, N., et al., "First Year Wilkinson Microwave Anisotropy Probe (WMAP), Observations On-Orbit Radiometer Characterization, ApJS 2003, 148, 29-37.

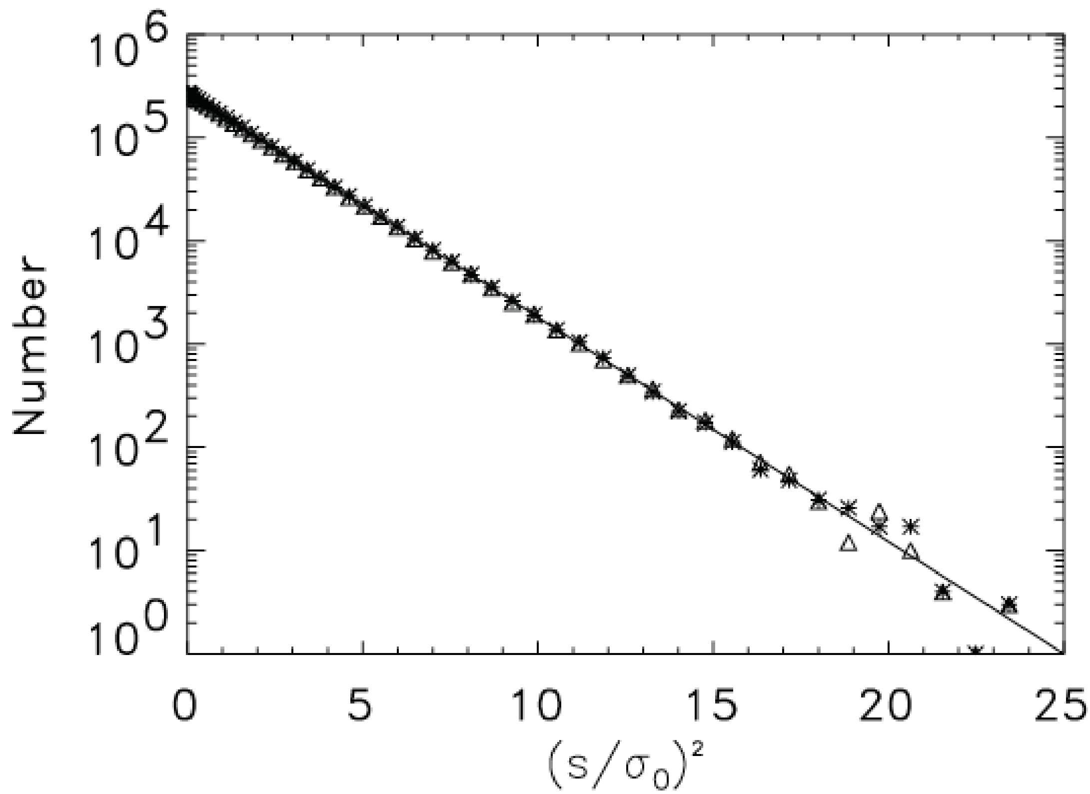

FIG. 6.—Distribution of the prewhitened V12 radiometer noise obtained from 10 days of observations. Sky signals arising from the dipole, CMB, and Galaxy have been removed. Data points were cut when either radiometer beam encountered a planet or a region of high Galactic emission. The line corresponds to a unit variance Gaussian distribution normalized to the observed frequency at $s = 0$. The two symbols denote the values obtained from the two sides of the distribution. The highly Gaussian distribution indicates that the noise variance for each pixel of the resulting sky maps should scale inversely with the number of observations of that pixel.

Jarosik, N., et al., "First Year Wilkinson Microwave Anisotropy Probe (WMAP), Observations On-Orbit Radiometer Characterization, ApJS 2003, 148, 29-37.

WMAP: 'First Light' Image

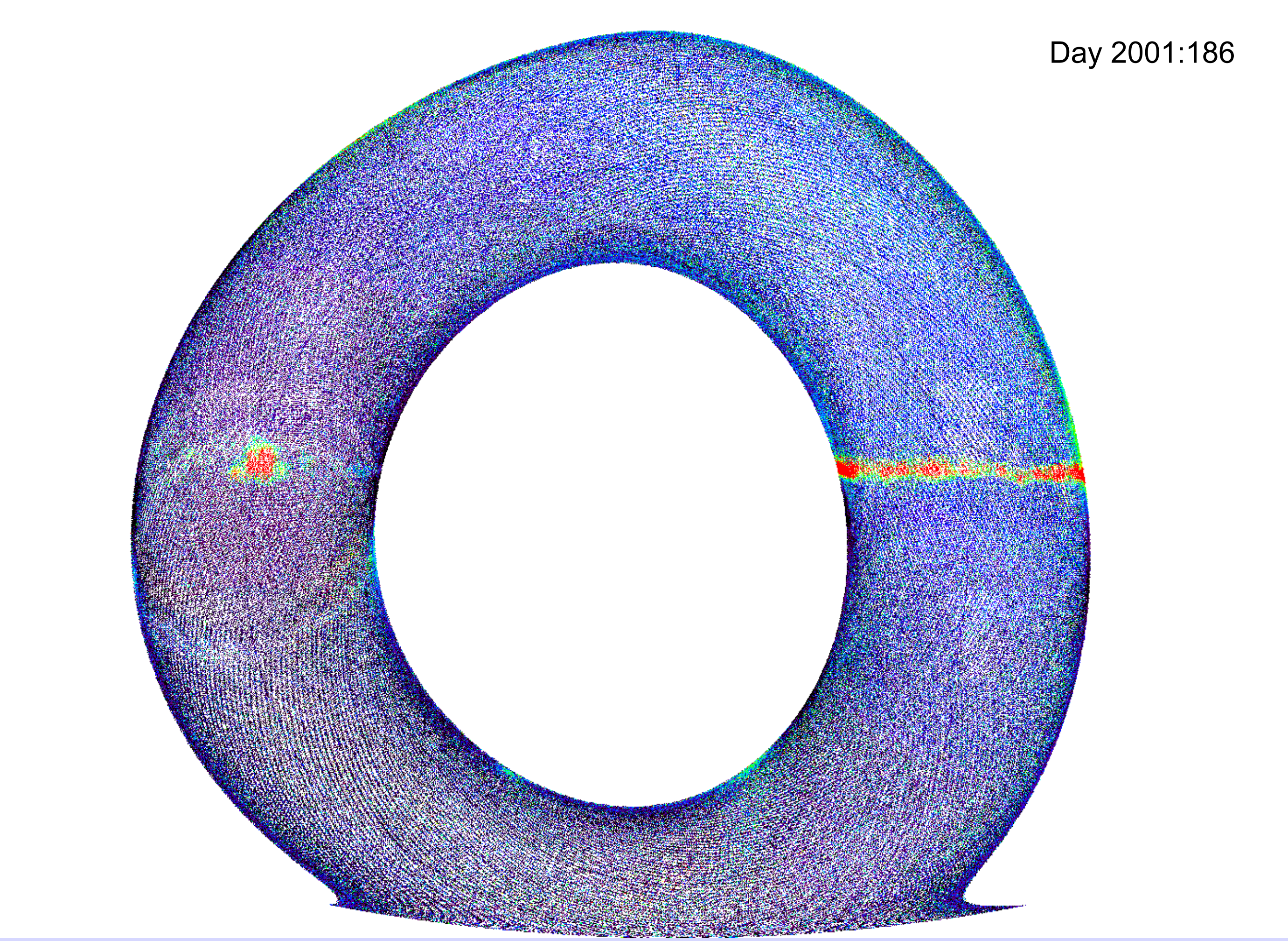

WMAP: Map-Making and Calibration

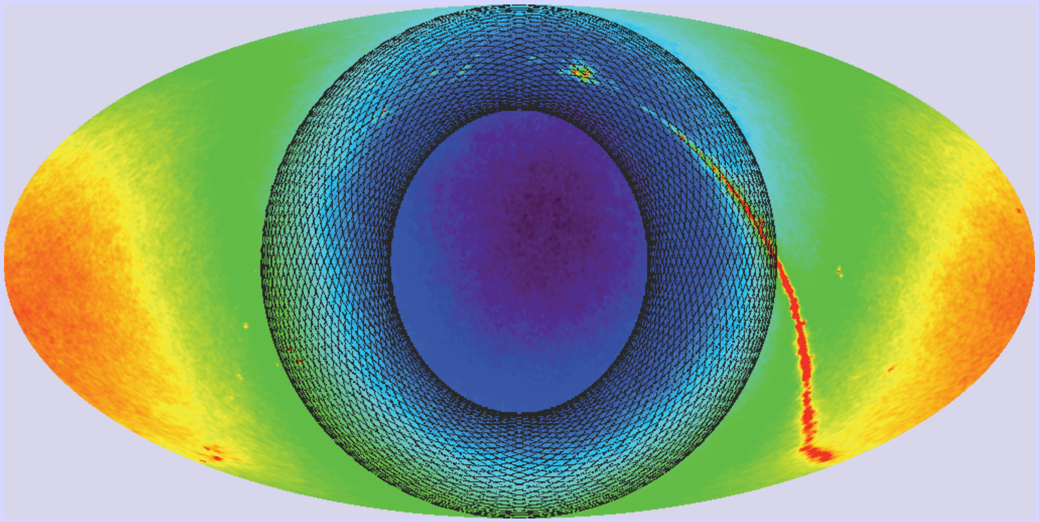

- Gain and baseline calibration based on known dipole modulation due to motion of WMAP around the Sun

- COBE dipole provides short-term transfer standard

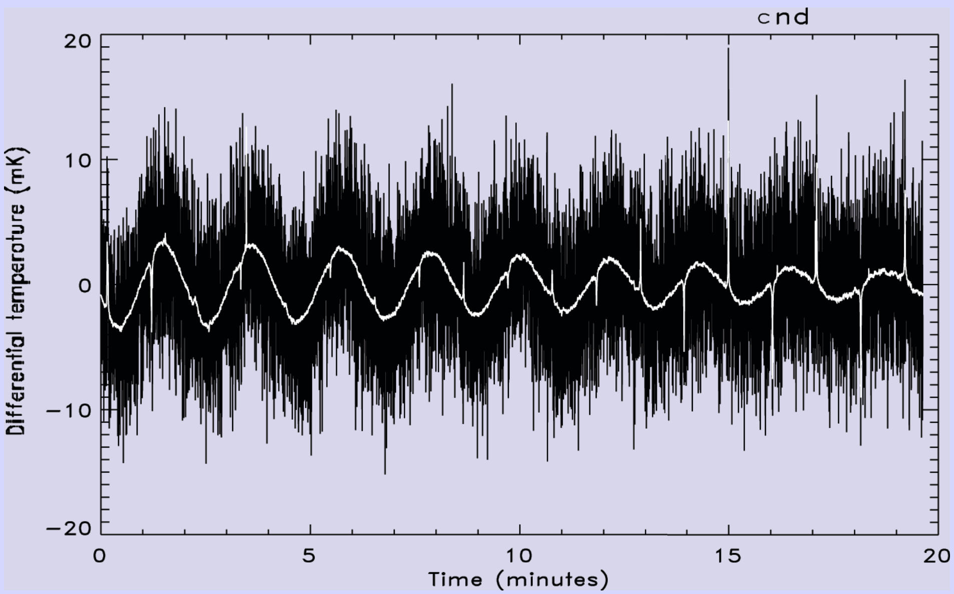

The degree of ***interconnection*** in the map and ***stability*** over the calibration time scale is a key to controlling the introduction of strips or other artifacts in the map…

WMAP: Improved Gain Model

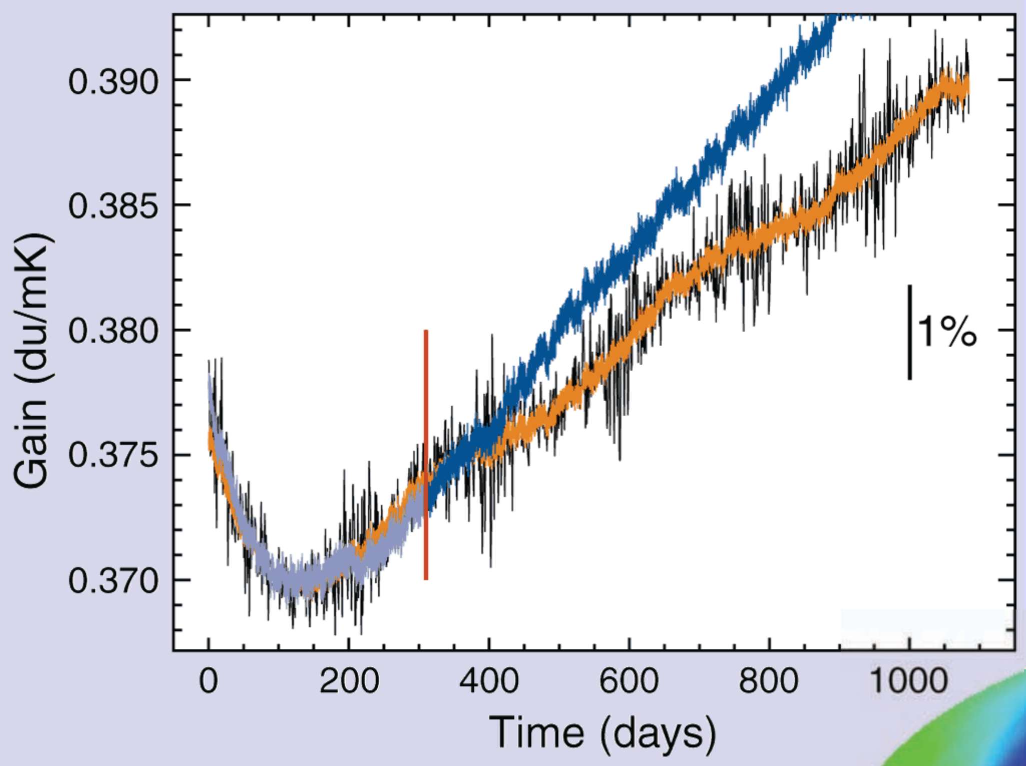

Left – instrument gain vs. time for 1-WMAP channel (V223).

Black: gain fit to dipole.

Grey/blue: model gain fit to 1st year data.

Orange: model 3-year data gain fit.

Right – difference between sky map solutions using above two model gain solutions, in ecliptic coordinates.

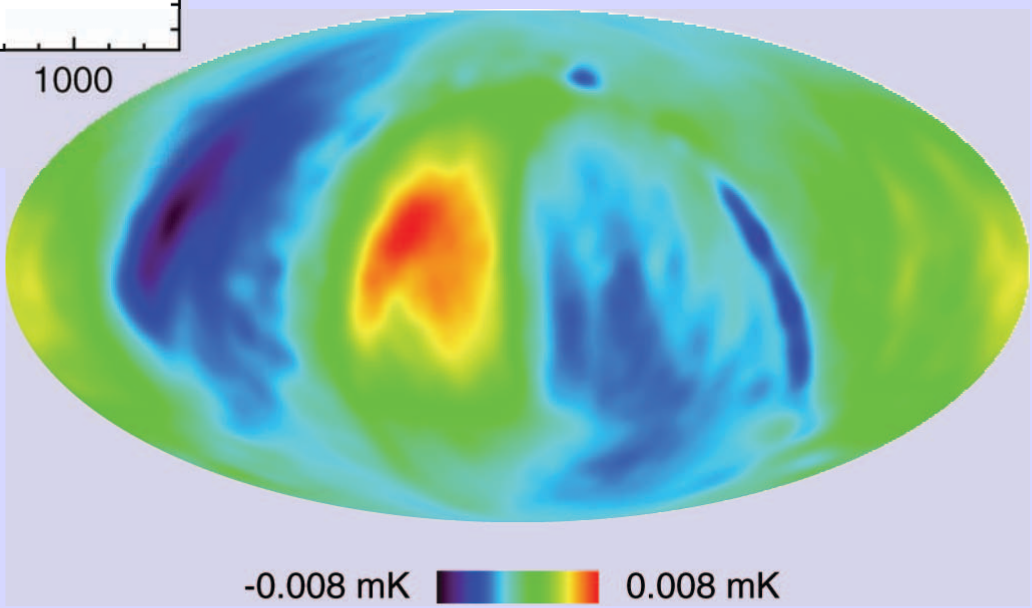

WMAP: 5-year Temperature Maps

23 GHz

33 GHz 61 GHz

41 GHz 94 GHz

Color scale: ±200 μK

Smoothing: 0.2° FWHM

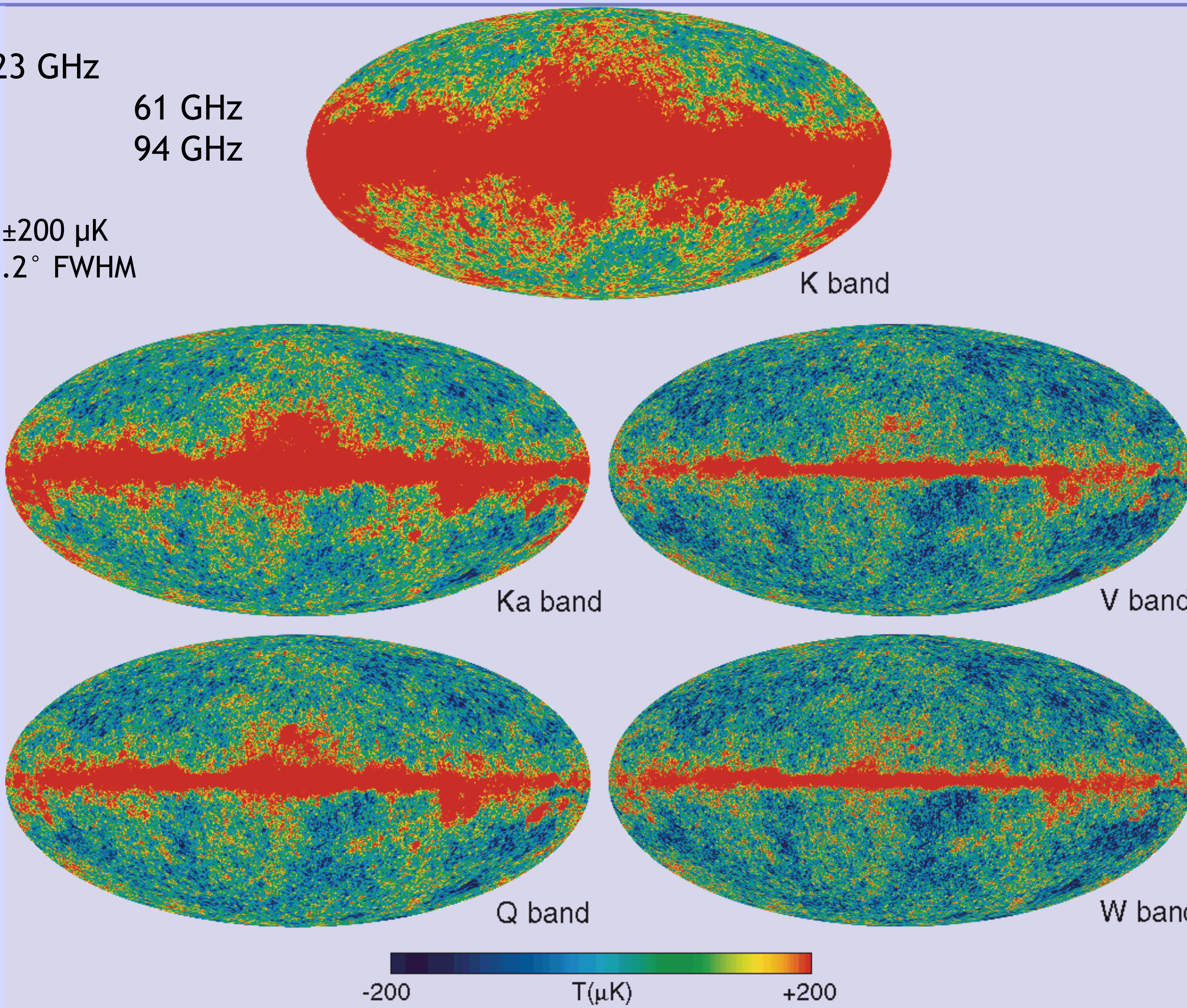

WMAP: 5-year Polarization Maps

Color: polarization intensity, smoothed to 2° FWHM

$$P = \sqrt{Q^2 + U^2}$$

Direction: shown for S/N>1

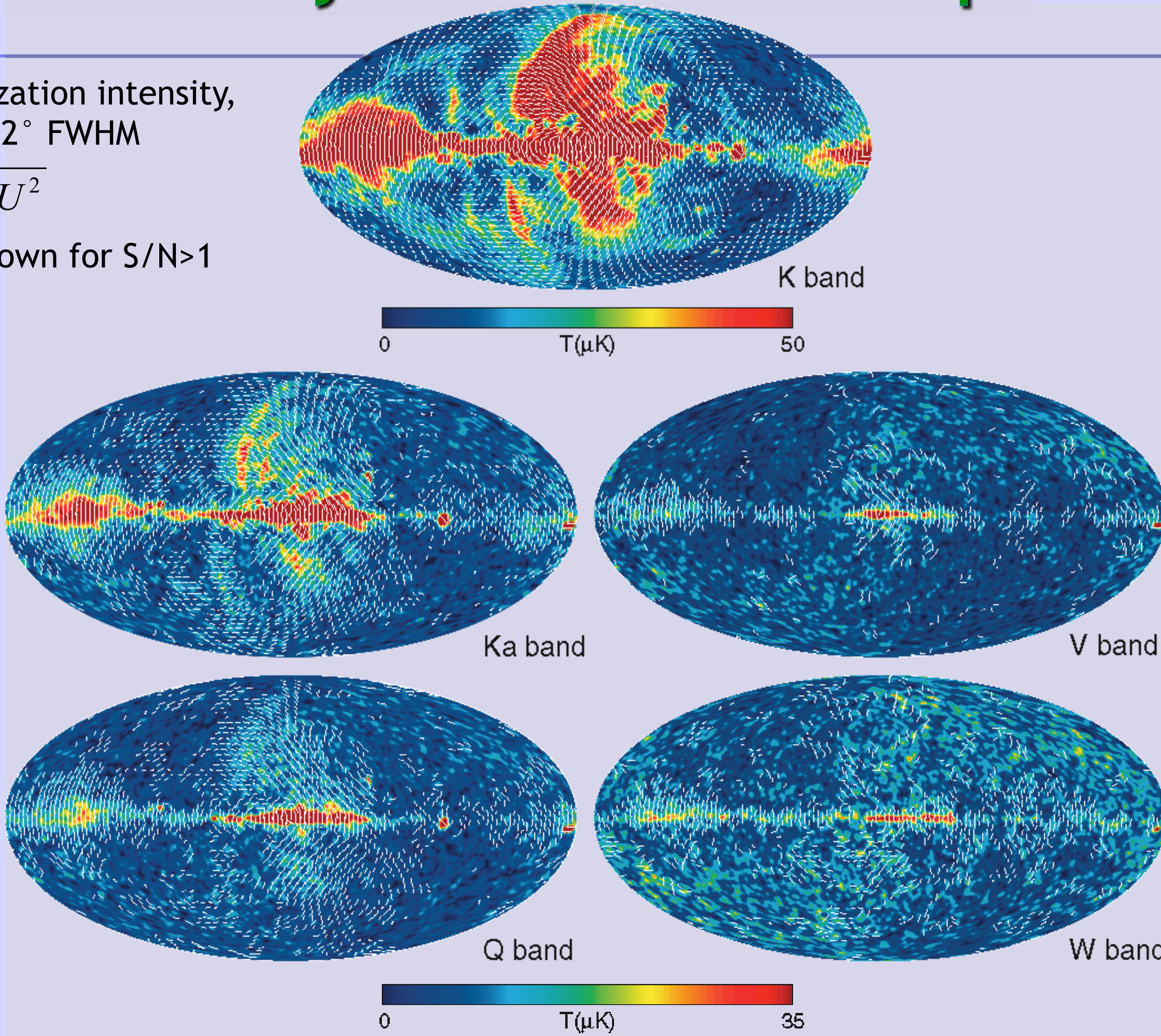

WMAP: ILC - 3-Color Maps

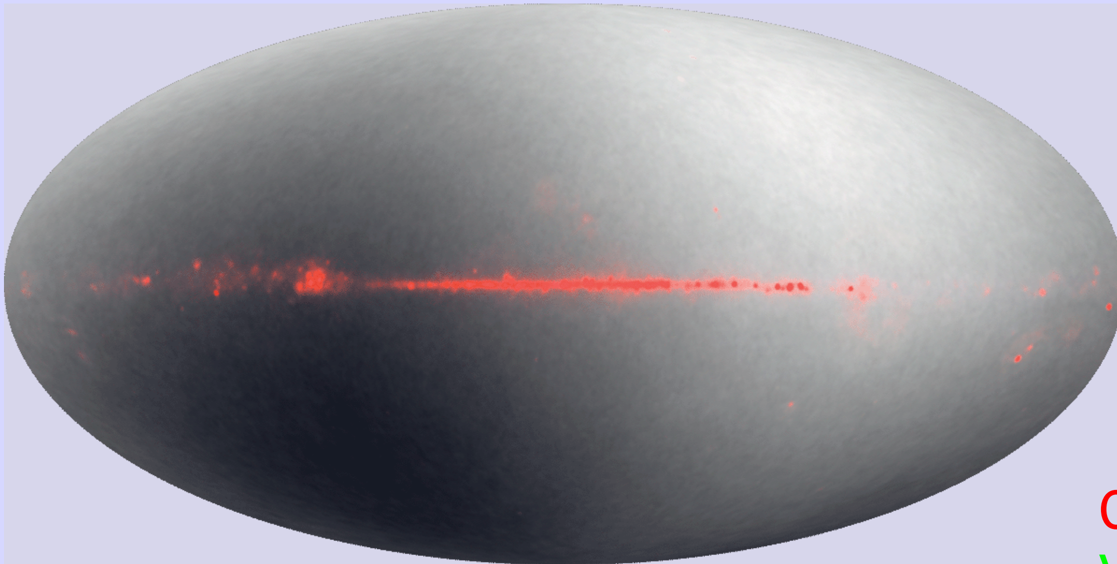

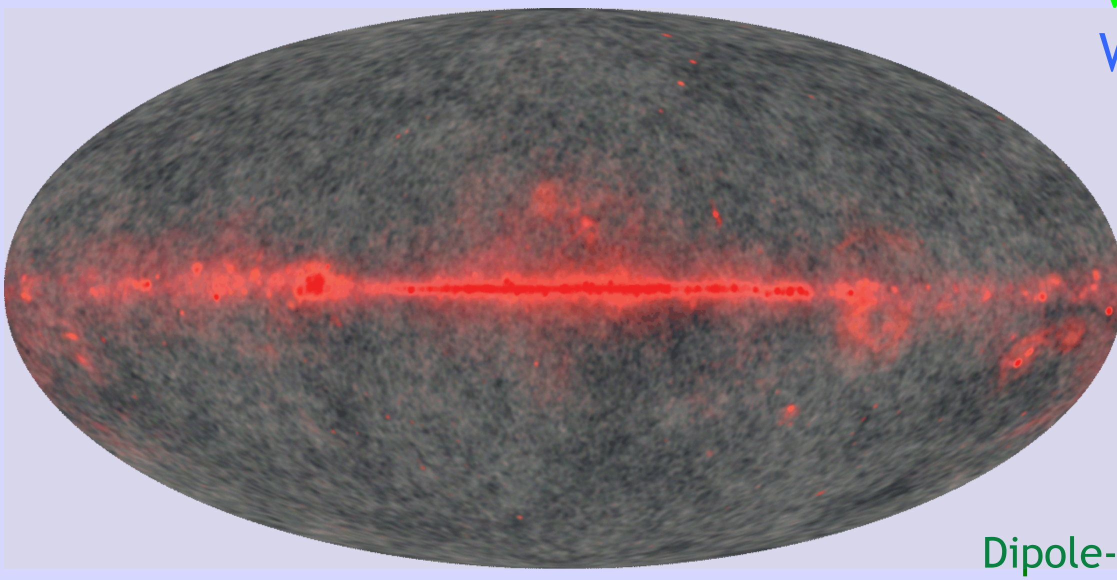

Q band
V band
W band

Dipole- subtracted

WMAP: ILC - CMB Temperature Anisotropy

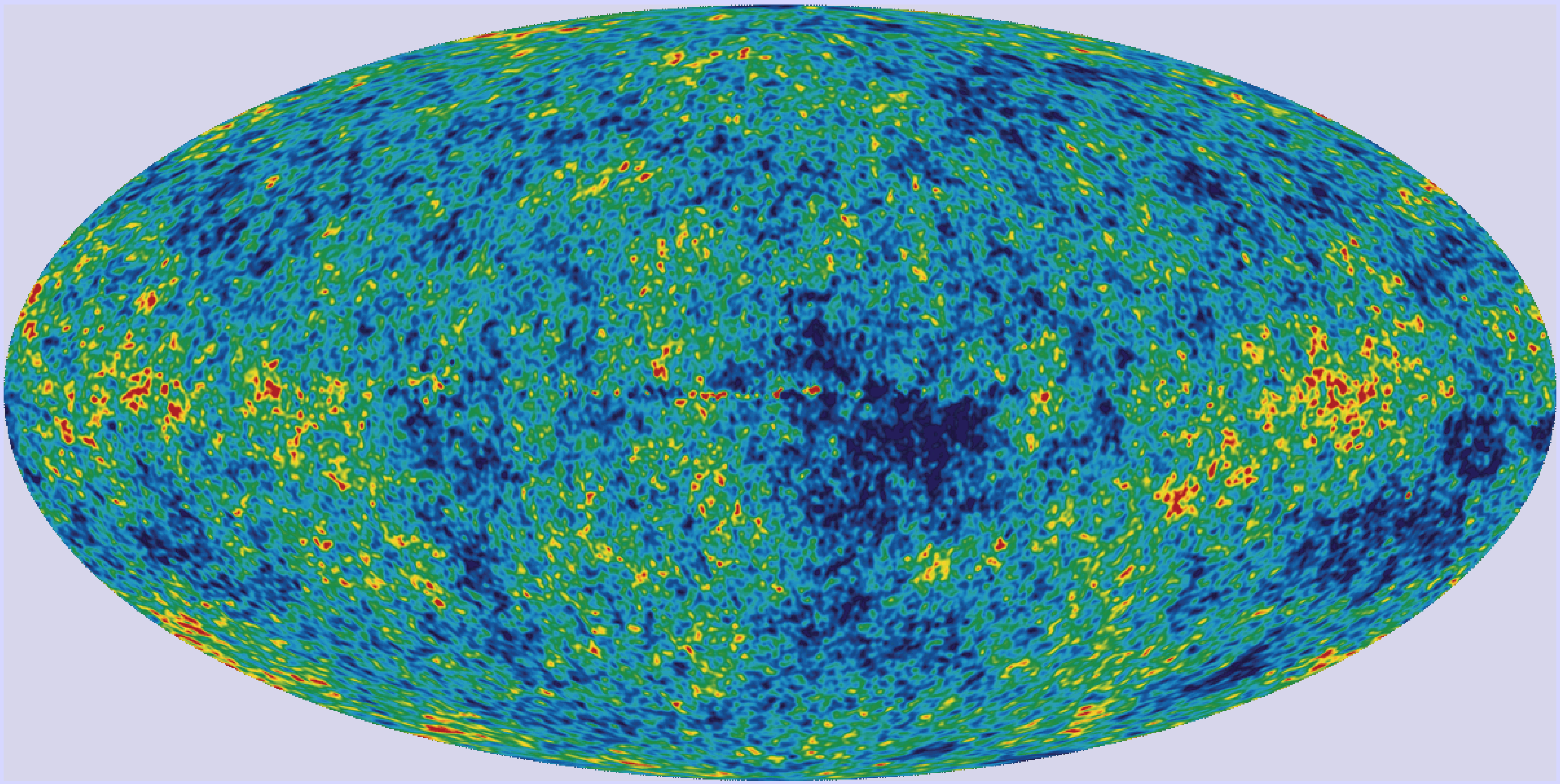

Consistent with a gaussian distribution and random phase…

NRAO: GBT Dual-Polarization Multi-Beam Receiver

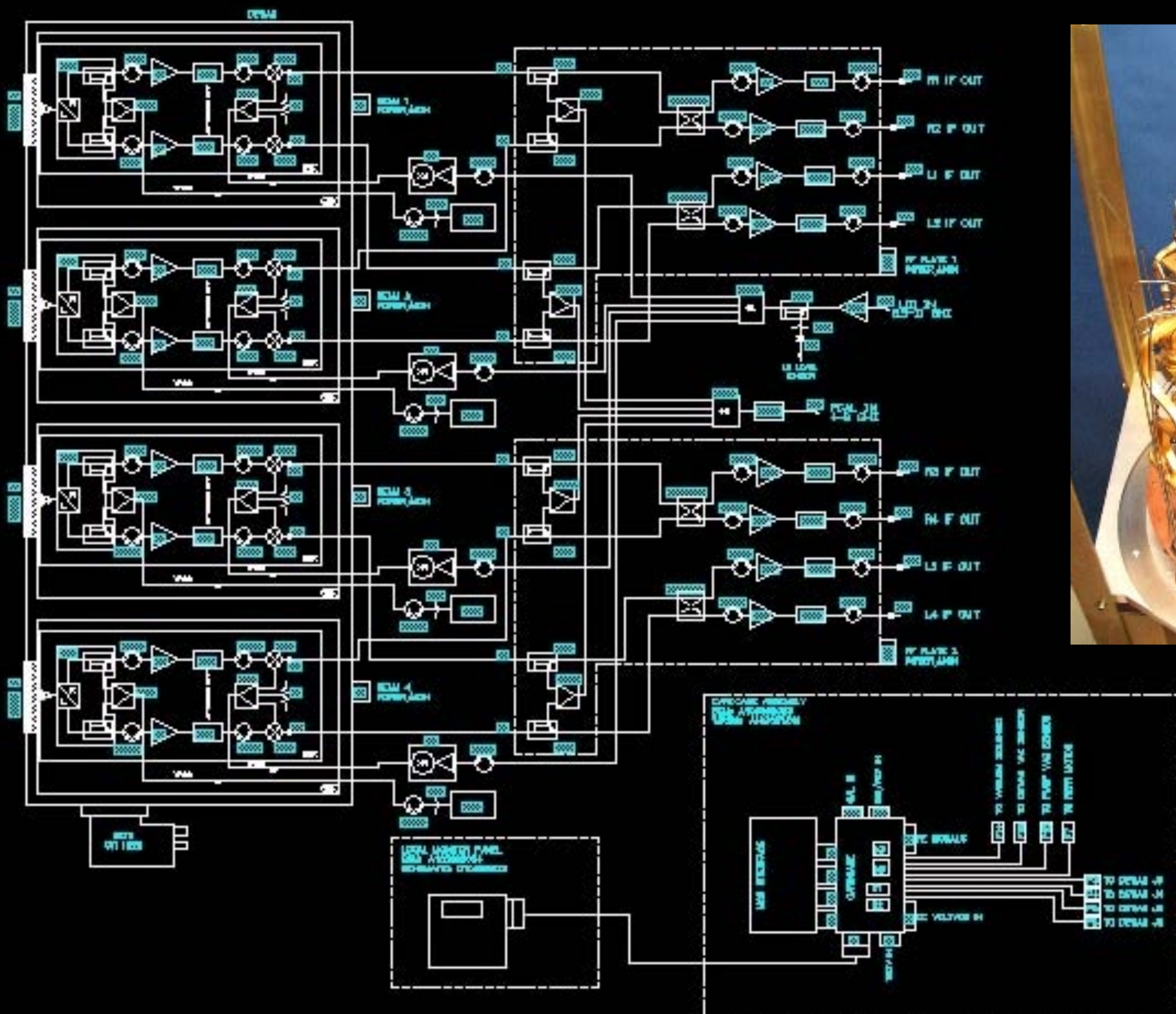

(Source: NRAO/GB)

Selected References – Noise, *'1/f'*, and Related Physical Processes

- M. W. Pospieszalski, "Modeling of Noise Parameters of MESFET's and MODFET's and Their Frequency and Temperature Dependence," 1989, IEEE Trans. Microwave Theory and Tech., Vol. MTT-37, pp. 1340-1350.
- M. W. Pospieszalski, et al., "Millimeter-Wave, Cryogenically-Coolable Amplifiers Using AlInAs/GaInAs/InP HEMTs", 1993, IEEE MTT-S Digest, pp. 515-518. (HEMT leakage current noise)
- B. Hughes, "A Temperature Noise Model for Extrinsic FET's," 1992, IEEE Trans. Microwave Theory Tech., vol. 40, pp. 1821–1831.
- R.F. Voss and J. Clarke, "Flicker (*1/f*) Noise: Equilibrium Temperature and Resistance Fluctuations", 1976, Physical Review B, Vol. 13, No. 2, pp. 556-573. (*1/f* in metal films)
- M.S. Keshner, "*1/f* Noise", 1982, Proc. IEEE, Vol. 70, No. 3, pp. 212-218. (Physically insightful)
- A. van der Ziel, "Noise in Solid State Devices and Circuits", 1986, Wiley, New York. (*1/f* survey)
- K. Kandiah, M.O. Deighton, F.B. Whiting, "A Physical Model for Random Telegraph Signal Current in Semiconductor Devices", 1989, J. Appl. Phys., Vol. 66, No. 2, pp. 937-948.
- G. Reimbold, "Modified *1/f* Trapping Noise Theory and Experiments in MOS Transistors Biased from Weak to Strong Inversion – Influence of Interface States", 1984, IEEE Transactions on Electron Devices, Vol. ED-31, No. 9, pp. 1190 – 1198.
- J.-M Peransin, et al., "*1/f* Noise in MODFET's at Low Drain Bias", 1990, IEEE Transactions on Electron Devices, Vol. 37, No. 10, pp. 2250-2253.
- A. Longoni, E. Gatti, R. Sacco, "Trapping Noise in Semiconductor Devices: A Method for Determining the Noise Spectrum as a Function of the Trap Position," 1995, J. Appl. Phys., Vol. 78, No. 10, pp. 6283-6297.
- H.C. Duran, et al., "Low-Frequency Noise Properties of Selectively Dry Etched InP HEMT", 1998, IEEE Transactions on Electron Devices, Vol. 45, No. 6, pp. 1219-1225.

Selected References – Receivers, Radiometers, and Stability

- R. Dicke, “The Measurement of Thermal Radiation at Microwave Frequencies,” 1946, Rev. Sci. Instrum., Vol. 17, No. 7, pp. 268-275.
- R. Hanbury-Brown, R.Q. Twiss, “A New Type of Interferometer for Use in Radio Astronomy,” 1954, Philosophical Mag., Vol. 45, No. 366, pp. 663-682.
- E.J. Blum, “Sensitivity of Correlation Radio Telescopes and Receivers,” 1959, Annales, D’ Astrophysique, Vol. 22, No. 2, p. 140.
- S. Weinreb, “Digital Radiometer,” 1961, Proc. IRE, Vol. 49, p. 1099..
- J. Hach, “Proposal for a Continuously Calibrated Radiometer,” 1966, Proc. IEEE, Vol. 54, pp. 2015-2016.
- G. Aitken, “The Multi-Correlation Receiver,” 1966, Proc. IEEE (Letters), Vol. 54, pp. 703—704; G. Aitken, “A New Correlation Radiometer,” 1968, IEEE Trans. Antennas and Propagation, Vol. 16, No. 2, pp. 224-228.
- J. Faris, “Sensitivity of a Correlation Radiometer,” 1967, J. Res. Nat. Bur. Stand., Engr. & Instr., Vol. 71C, pp.153-170.
- J. Hach, “A Very Sensitive Airborne Microwave Radiometer Using Two Reference Temperatures,” 1968, IEEE Transactions Microwave Theory and Techniques, Vol. 16, No. 9, pp. 629-636.
- M.S. Hersman and G.A. Poe, “Sensitivity of the Total Power Radiometer with Periodic Absolute Calibration”, 1981, IEEE Trans. Microwave Theory and Techniques, Vol. 29, No. 1, pp. 32-40.
- C.R. Predmore, et al., “A Continuous Comparison Radiometer at 97GHz,” 1985, IEEE Trans. on Microwave Theory and Techniques, Vol. 33, No. 1, pp. 44-51.
- S. Padin, “A Wideband Analog Continuum Correlator for Radio Astronomy,” 1994, IEEE Trans. Instrum. and Measurement, Vol. 43, No. 6., pp. 782-785.

A (Very) Brief FET History…

1930	Lilienfeld	**TRANS**fer-res**ISTOR** concept proposed **F**ield-**E**ffect-**T**ransistor (**FET**)
1947	Bardeen, Brattain, and Shockley (Bell Telephone Laboratories)	Bi-polar transistor invented **B**i-polar-**J**unction-**T**ransistor (**BJT**)
1952	Shockley (Bell Telephone Laboratories)	Uni-polar transistor concept analyzed **J**unction-**F**ield-**E**ffect-**T**ransistor (**JFET**)
1966	Mead (California Institute of Technology)	Device structure proposed **ME**tal-**S**emiconductor-**FET** (**MESFET**)
1967	Hooper and Lehrer (Fairchild Semiconductor)	First MESFET fabricated on GaAs (T_n~450K @ 1 GHz; T_a=300K)
1970	Esaki, and Tsu (IBM) Loriou, Bellec, Le Rouzic (National Telecommunications Center, France)	Prediction of carrier accumulation at hetrointerface Early investigations of cooled MESFET amplifiers (T_n~120K @ 1 GHz; T_a=77K)
1975	Pucel, Haus, and Statz (Raytheon)	"PRC" FET noise model presented
1978	Dingle, Stormer, Gossard, and Wiegmann (AT&T Bell Laboratory)	Accumulation of carriers and increase in electron mobility at hetrointerface demonstrated
1979	Fukui (AT&T Bell Laboratories)	Fukui scaling laws proposed for FETs
1980	Weinreb (NRAO) Mimura, Hiyamizu, Fuji, and Nanbu (Fujitsu Laboratories, Japan) (Bell Laboratories) (Thomson-CSF, France) (U of IL / Rockwell International)	Practical cryogenic FET amplifiers demonstrated First hetrojunction field effect transistor reported **H**igh-**E**lectron-**M**obility-**T**ransistor (**HEMT**) **S**electively-**D**oped-**H**etrojuntion-**T**ransistor (**SDHT**) **T**wo-dimensional-**E**lectron-**G**as-**FET** (**TEGFET**) **MO**dulation-**D**oped-**FET** (**MODFET**)
1982	Delagebeaudeuf and Lihn (Thomson-CSF, France)	Device design analysis presented for HFETs
1989	Pospieszalski (NRAO)	"Tg/Td" HFET noise model presented
2000	**State of the Art…** (Hughes, TRW, JPL, …)	→ GaAs HFETs (T_n~3K @ 1 GHz; T_a=4K) → InP HFET MMICs (>100 GHz)

Field Effect Transfer-Resistor:

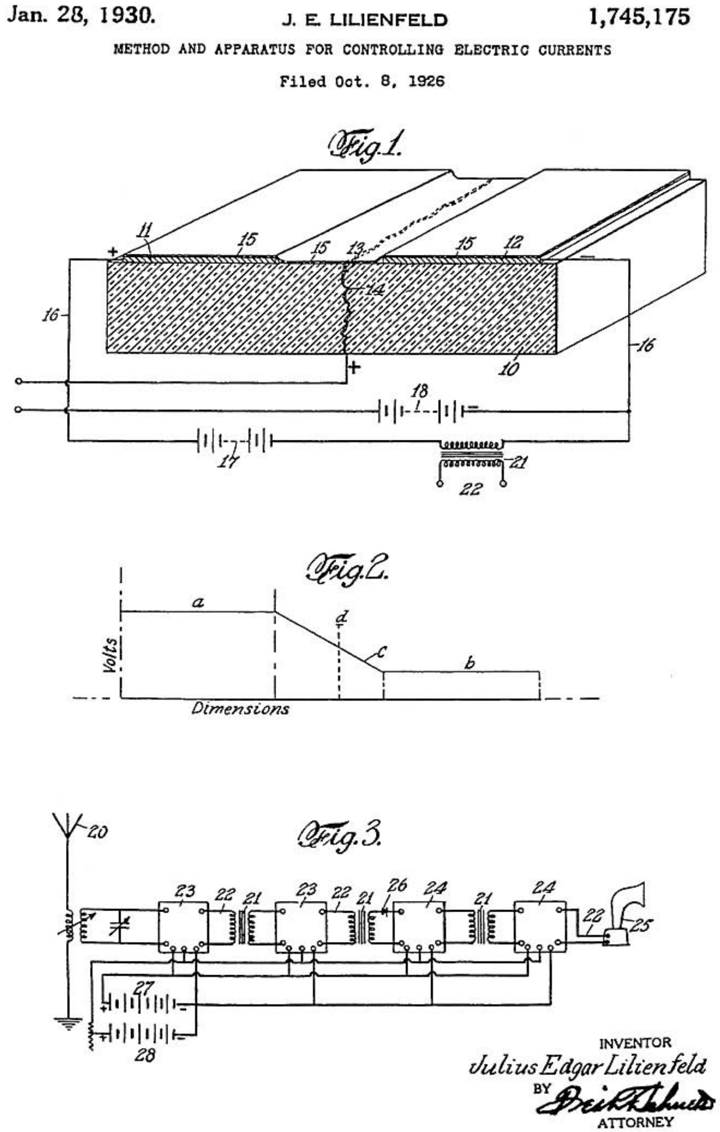

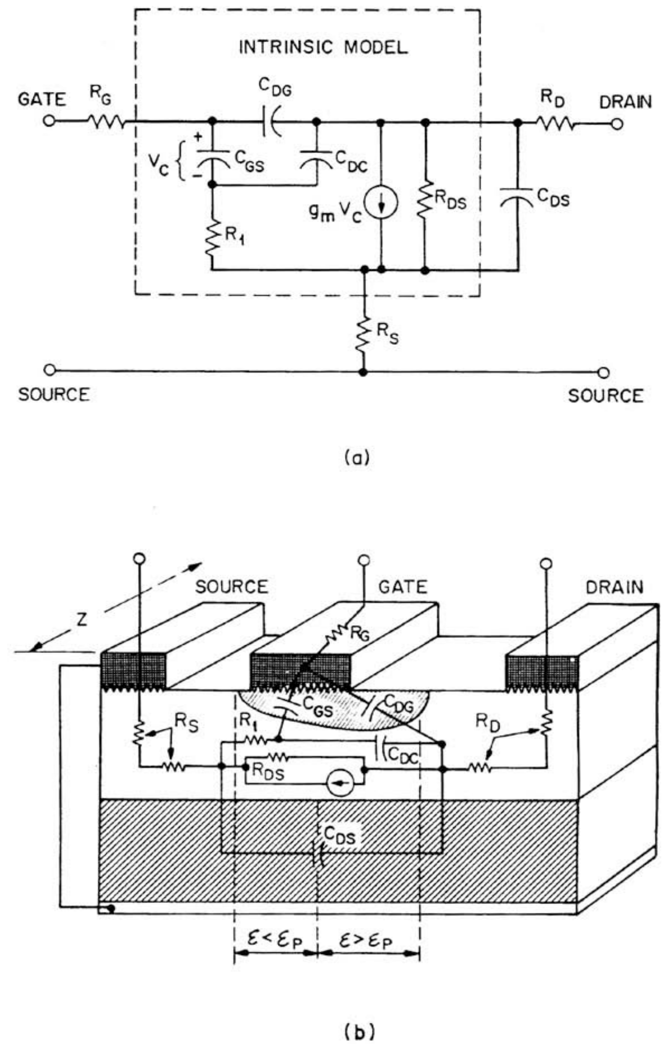

Fig. 20 (a) Equivalent circuit of a MESFET and (b) physical origin of the circuit elements. (After Liechti, Ref. 8.)

Schockley Field Effect Transistor Model:

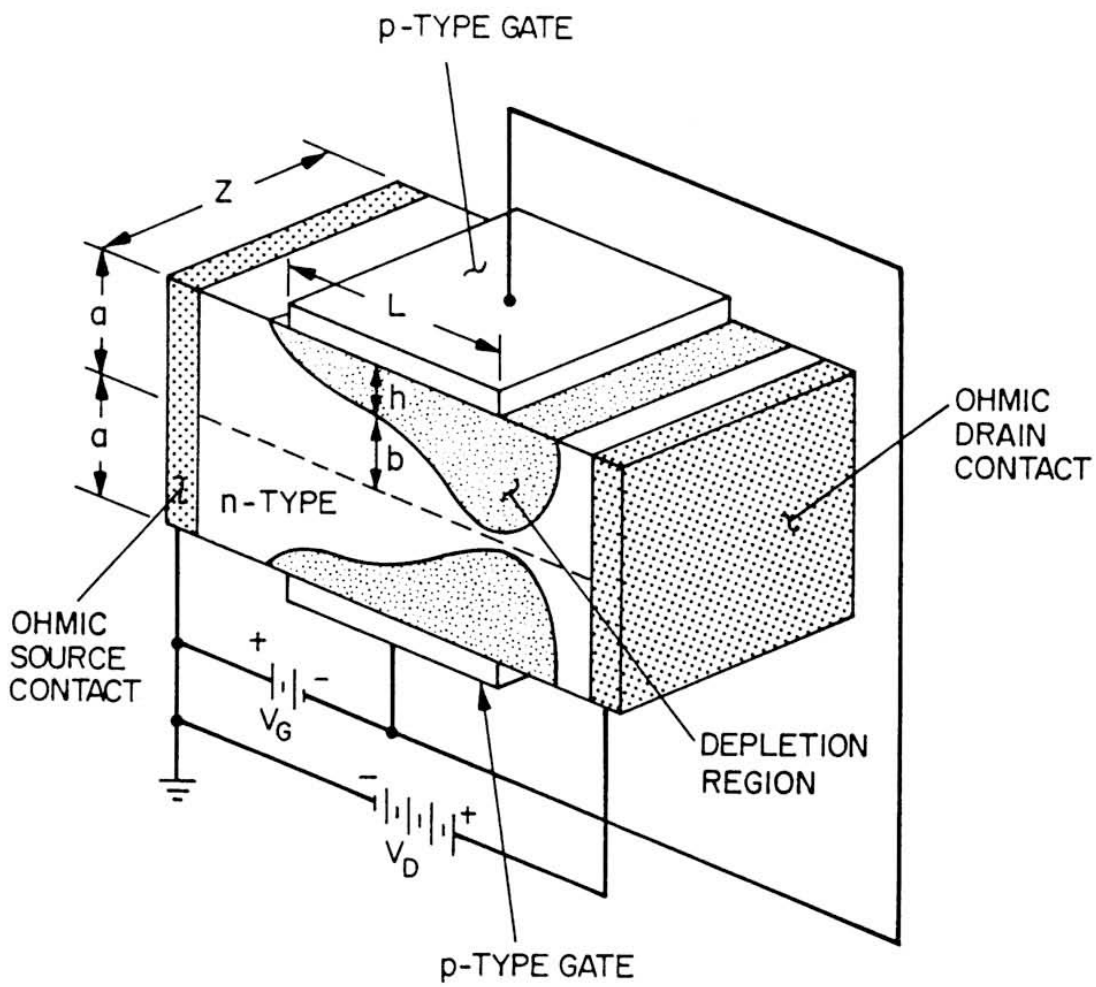

Shocklev's model of the iunction field-effect transistor. (After Dacev and Ross.